A two-step geospace storm as a new tool of opportunity for experimentally estimating the threshold condition for the formation of a substorm current wedge

Leonid F. Chernogor

Department of Space Radio Physics, V. N. Karazin Kharkiv National University, Kharkiv, 61022, Ukraine

Correspondence to: Leonid Chernogor (e-mail: Leonid.F.Chernogor@gmail.com)

Abstract. In the study of coupling processes acting within the upper atmosphere, a major challenge remains in quantifying the transformation of energy. One of the energy pathways between the ionospheric heights and the magnetosphere is the diversion of the cross-tail electric current into the ionosphere through the current wedge. One of the most interesting observations made in this study shows that, during one of the two steps of the two-step storm, part of the near-Earth cross-tail current closed itself via the ionosphere, to which it was linked by the substorm current wedge, and manifested itself in the magnetograms acquired at high and equatorial latitude stations on the night side of the Earth. As result, the two-step character of this storm has allowed us to suggest that the B_z interplanetary magnetic field component threshold for the formation of the substorm current wedge lies within the –(22–30) nT interval. Consequently, this study suggests, for the first time, that the emergence of a current wedge during a two-step geospace storm may be quantified by a threshold value of the interplanetary magnetic field (IMF) B_z component utilizing observations made during a two-step geospace storm with ground-based magnetometers. The study, for the first time, convincingly attest to the two-step geospace storm to be an ideal solar-terrestrial event of opportunity for realizing a technique for estimating the IMF B_z component threshold for the formation of the substorm current wedge. These conclusions have been drawn from the examination of the latitudinal dependence of variations in the geomagnetic field on the surface of the Earth on the global scale during the severe two-step geomagnetic storm of 23–24 April 2023, a major two-step storm in solar cycle 25. The data available at INTERMAGNET magnetometer network URL (https://imag-data.bgs.ac.uk/GIN_V1/GINForms2) were chosen for two near-meridional chains of stations, one in the western (eight stations) and the other in the eastern (ten stations) hemispheres, which were situated, for the first time, in such a way that one of them was in the night hemisphere during both of the two steps of the geomagnetic storm. Other features of this two-step storm include the following. In the western hemisphere, the fluctuations of the geomagnetic field strength on the days used as a quiet time reference period usually did not exceed a few tens of nanotesla (nT), whereas in the course of the disturbed days, the variations in the geomagnetic field strength increased by a factor of 2 to 10 and reached a few hundred nT. In the eastern hemisphere during quiet times, the middle and low latitude magnetometer stations generally recorded strength fluctuations smaller than 10–20 nT, while during the disturbed period the fluctuations increased by a factor of 2–5 and greater, attaining ±(50–70) nT. The strength fluctuations showed a considerable, up to 300–700 nT, increase at high latitudes. The northward component of the geomagnetic field, X, exhibited the greatest perturbations

35   at all latitudes in both hemispheres, as the level of strength fluctuations decreased with decreasing latitude. The

36   geomagnetic field strength fluctuations recorded at the magnetometer stations nearly-equidistant from the equator

37   were observed to be close in magnitude. Close in value also were the strength fluctuations observed with the stations

38   at close latitudes but in different hemispheres.

1 Introduction

40   Solar storms accompanied by solar flares, coronal mass ejections, the generation of shocks associated with coronal

41   mass ejections or fast solar wind streams, act to generate a complex set of processes in the solar-terrestrial system

42   comprised of the sun, interplanetary medium, magnetosphere, ionosphere, atmosphere, and solid earth to produce

43   geospace storms or to cause significant variations in space weather. A geospace storm includes synergistically

44   interacting storms in the magnetic field (geomagnetic storms), in the ionosphere (ionospheric storms), in

45   thermospheric neutral density variations, earlier termed the thermospheric storms (see, e.g., (Prölss and Roemer,

46   1987)), in the electric field in the magnetosphere, ionosphere, and atmosphere (electrical storms) (see, e.g.,

47   (Kleimenova et al., 2008; Chernogor and Domnin, 2014; Kleimenova et al., 2017; Chernogor, 2021a). Geospace

48   storms actually constitute the state of space weather. Space weather can have adverse effects on ground systems,

49   such as radars or power lines (effects involving magnetic-storm-induced geoelectrical currents), or space-, air-, and

50   ground-based communication links. The latter include errors in Global Positioning System and VLF navigation

51   systems, loss of HF communications (Wang et al., 2022; Wang et al., 2023), disruption of UHF satellite links due to

52   scintillations, etc. Disturbances appear in all ranges of radio waves, from VLF to UHF. Thus, many of humankind's

53   technological systems are susceptible to failure or unreliable performance because of geospace storms, and therefore

54   the study of the manifestations of geospace storms in all geospheres and geophysical fields remains an important

55   task.

56

57   The manifestations of geomagnetic storms have been studied better than those of the other kinds of storms. They are

58   dealt with in a large number of studies concerned with a major challenge to quantify the energetics of magnetic

59   storms (see, e.g., (Gonzalez et al., 1994)), the geomagnetic storm effects within the altitude range from the Earth's

60   surface to 100km at milatitudes (see, e.g., (Laštovička, 1996)), the thermospheric response to geomagnetic activity

61   on a global scale (see, e.g., (Fuller-Rowell et al. (1997) and Buonsanto (1999)), the ionospheric response to

62   magnetic storms (see, e.g., (Danilov and Laštovička, 2001)), the dynamic processes in the ionosphere during

63   magnetic storms from the Kharkov incoherent scatter radar observations (Chernogor et al., 2007), the statistical

64   characteristics of geomagnetic storms in the 24th cycle (Chernogor, 2021b), the origin of dawnside subauroral

65   polarization streams during major geomagnetic storms (Lin et al., 2022), the simulation of a total of 122 storms

66   ground magnetic variations, from the period 2010–2019, which has shown that high-latitude regional disturbances

67   are still difficult to predict (Al Shidi et al., 2022), and nonlinearities in the ionosphere and thermosphere response to

68   forcing uncertainties (Hsu and Pedatella, 2023). Since a myriad of geomagnetic storm manifestations may be

69   observed, these issues have been summarized from time to time in books. They include a comprehensive discussion

70   of ionospheric F-region storms (Prölss, 1995); the most recent developments in space weather (Daglis, 2001); a

71 comprehensive overview of space weather (Song et al., 2001); scientific background of space storms for explaining

72 magnetic storms on earth (Bothmer and Daglis, 2006); the importance of the tail current (Kamide and Maltsev,

73 2007); key concepts of space weather (Moldwin, 2022); and the current state of the art in the field of space storms

74 (Koskinen, 2011). The main concern was to study the most severe storms, since they have the strongest impact on

75 human well-being and the correct functioning of space- and ground-based systems and can affect human health. The

76 latter include space weather, which can endanger human life or health directly (e.g., (Daglis, 2001; Song et al.,

77 2001)); biological impacts of space storms (Bothmer and Daglis, 2006), and the perils of living in space generally

78 (Moldwin, 2022).

79

80 Only one of many magnetic storms, a solar cycle 24 major storm of September 2017, was concerned with in dozens

81 of studies, which were devoted to geomagnetic storm effects on the thermosphere and ionosphere (see, e.g., (Qian et

82 al., 2019); latitudinal dependence of quasi-periodic variations in the geomagnetic field Chernogor and Shevelev,

83 2020); negative ionospheric response over the European sector (Oikonomou et al., 2022); ionospheric storm over the

84 Brazilian and African longitudes (Fagundes et al., 2023)). Examples of other magnetic storms that occurred over

85 2016–2022 include physics of geospace storms (Chernogor, 2021a); the statistical characteristics of geomagnetic

86 storms in the 24th cycle of solar activity (Chernogor, 2021b); the effects of the strong ionospheric storm of August

87 26, 2018 as captured with multipath radio wave monitoring (Chernogor et al., 2021); the incoherent scatter radar and

88 ionosonde observations of the ionospheric storm of 21–24 December 2016 (Katsko et al., 2021); the influence on

89 high frequency radio wave characteristics of dynamic processes in the magnetic field and in the ionosphere during

90 the 30 August-2 September 2019 geospace storm (Luo et al., 2021a); the geospace storm effects on 5–6 August

91 2019 (Luo et al., 2021b); magneto-ionospheric effects of the geospace storm of 21–23 March 2017 (Luo et al.,

92 2022); characteristic features of the magnetic and ionospheric storms of 21–24 December 2016 (Luo and

93 Chernogor, 2022); thermospheric temperature and density variability during the 3–4 February 2022 minor

94 geomagnetic storm (Laskar et al., 2023). The statistical analysis of geomagnetic storm effects can be found in

95 (Chernogor, 2021b; Abe et al., 2023; De Abreu et al., 2023).

96

97 The study of geomagnetic storms remains one of the main problems in space physics. This occurs for a few reasons.

98 First, every magnetic storm has its own individual features, in addition to the general characteristics. Second, the

99 manifestation of magnetic storms is dependent on the solar storm parameters and features, the general state of space

100 weather, geographic coordinates, local time, and solar cycle phase. The purpose of this paper is to analyze

101 characteristic features of latitudinal manifestations of the 23–24 April 2023 geomagnetic storm, a major two-step

102 storm in solar cycle 25 to date. The main features of the coronal mass ejection that caused this two-step storm can be

103 summarized as follows (Ghag et al., 2024). First, the storm lacked sudden storm commencement. Instead, the

104 interplanetary magnetic field B_z component turned southward at 17:37 UT on 23 April 2023 and remained negative

105 for about three hours, after which B_z was fluctuating during the sheath transit till almost 01:00 UT on 24 April 2023

106 with $B_z \sim -22$ nT (https://spaceweather.com/images2023/25apr23/cmeimpact.jpg). This process was the likely cause

107 of the first step of the severe geomagnetic storm. Next, a magnetic cloud transit occurred, with $B_z \sim -30$ nT, which

108 was the cause of the second step of the storm under study. The two magnetometer chains employed in this study
109 were chosen, for the first time, in such a way that one of them was in the night hemisphere of the Earth during both
110 of the two steps of the 23–24 April 2023 geomagnetic storm.

111

112 The paper begins with a description of the data being analyzed and the state of space weather. Next, the main results
113 of data analysis presented in Appendix in detail are summarized, and the diversion of the cross-tail current into the
114 ionosphere through a current wedge identified. Then the specification of a threshold for the emergence of the current
115 wedge is described, and the principle achievement of this study, which, for the first time, convincingly attest to the
116 two-step geospace storm to be an ideal solar-terrestrial event of opportunity for realizing a technique for estimating
117 the interplanetary magnetic field (IMF) B_z component threshold for the formation of the substorm current wedge.
118 The paper ends with the conclusions drawn.

119 **2 Data and materials**

120 The data available at INTERMAGNET magnetometer network URL (https://imag-
121 data.bgs.ac.uk/GIN_V1/GINForms2; retrieved 22 November 2023) from two near-meridional chains of stations, one
122 in the western (eight stations) and the other in the eastern (ten stations) hemispheres, have been retrieved (Fig. 1).
123 The vector magnetometers acquire measurements with 0.1-nanotesla (nT) strength resolution at a sampling rate of
124 one sample per second. The observatories in the western hemisphere are listed in Table 1 and those in the eastern
125 hemisphere are presented in Table 2. Analysis of temporal variations in the strength of the northward, X, eastward,
126 Y, and vertical, Z, components of the geomagnetic field over the period 20–26 April 2023 has been performed.

127

128 The data processing technique is as follows. First, the data on the absolute value of time variations are used to
129 calculate the diurnal trend. Then, the diurnal trend is subtracted from the primary time series resulting in the time
130 series of relative magnitudes. The relative magnitudes of variations in all components of the geomagnetic field are
131 subjected to further analysis.
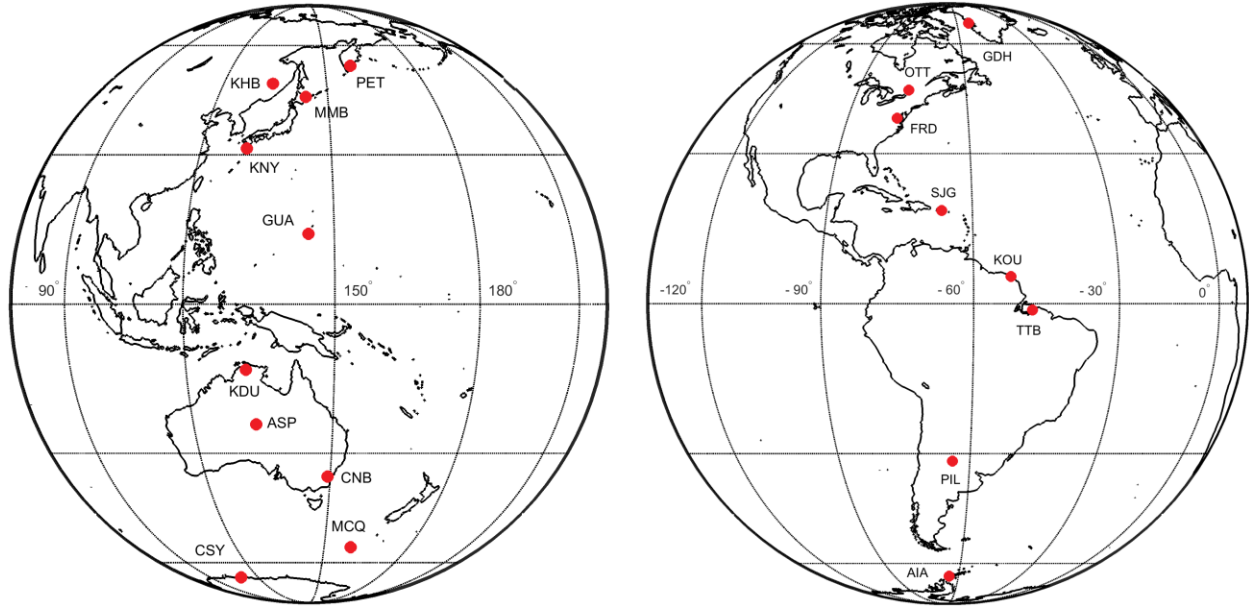
Figure 1: Map showing the recording stations.

Table 1 Observatories in the western hemisphere.

IAGA code, name, country	Geographic*		Corrected Geomagnetic*	
	Lat.	Long.	Lat.	Long.
GDH, Godhavn, Greenland	69.251°N	306.471°E	74.11°N	36.89°E
OTT, Ottawa, Canada	45.403°N	284.448°E	53.88°N	2.94°E
FRD, Fredericksburg, United States of America	38.205°N	282.627°E	47.13°N	359.97°E
SJG, San Juan, United States of America	18.111°N	293.85°E	25.23°N	12.27°E
KOU, Kourou, French Guiana**	5.209°N	307.267°E	13.99°N	20.49°E
TTB, Tatuoca, Brazil**	−1.201°N	311.494°E	7.37°N	24.38°E
PIL, Pilar, Argentina	−31.667°N	296.117°E	−21.13°N	5.43°E
AIA, Akademik Vernadsky, Antarctica	−65.246°N	295.743°E	−51.06°N	9.27°E

* The coordinates are retrieved from the list of geomagnetic observatories at
https://isgi.unistra.fr/listobs_index.php?index=SSC.
** The geomagnetic coordinates are not corrected.

Table 2 Observatories in the eastern hemisphere.

IAGA code, name, country	Geographic		Geomagnetic	
	Lat.	Long.	Lat.	Long.
PET, Paratunka (Petropavlovsk), Russian Federation	52.971°N	158.248°E	46.71°N	228.5°E
KHB, Khabarovsk, Russian Federation	47.61°N	134.69°E	41.65°N	208.57°E
MMB, Memambetsu, Japan	43.91°N	144.189°E	37.29°N	217.11°E
KNY, Kanoya, Japan	31.425°N	130.88°E	25.04°N	204.35 °E
GUA, Guam, United States of America	13.59°N	144.87°E	6.28°N	217.04°E
KDU, Kakadu, Australia	−12.686°N	132.472°E	−21.46°N	204.44°E
ASP, Alice Springs, Australia	−23.76°N	133.885°E	−33.53°N	207.84°E
CNB, Canberra, Australia	−35.313°N	149.364°E	−44.98°N	227.56°E

MCQ, Australia	−54.5°N	158.935°E	−63.92°N	248.84°E
CSY, Casey Station, Australia	−66.282°N	110.528°E	−80.49°N	159.89°E

* The coordinates are retrieved from the list of geomagnetic observatories at

https://isgi.unistra.fr/listobs_index.php?index=SSC.

3 Space weather

The data involved in the analysis of space weather include the temporal variations of solar wind parameters

(https://omniweb.gsfc.nasa.gov/form/dx1.html), the interplanetary magnetic field, the storm-time variation, D_{st}, and

the three-hour planetary, K_p, indices (https://wdc.kugi.kyoto-u.ac.jp/), as well as calculated solar wind dynamic

pressure and the Akasofu energy function, all of which are presented in Fig. 2.

During the 23–24 April 2023 storm, the solar wind showed a peak in the proton density of 21.1×10^6 m^{-3} from a

background of $(5–10) \times 10^6$ m^{-3}, when the solar wind speed exhibited an enhancement to 706 km/s from a

background of 350–400 km/s observed prior to the storm. These enhancements were accompanied by a rise in the

dynamic pressure of 11 nPa from a background of 1–3 nPa, and by an increase in the temperature of 20.5×10^5 K

from a background of $(1–2) \times 10^5$ K. Under quiet conditions, the strengths of the IMF B_y and B_z components usually

did not exceed ±5 nT, whereas they significantly increased on 23 and 24 April 2023, with $B_{y\max} \approx 9.5$ nT, $B_{y\min} \approx -$

30.2 nT, $B_{z\max} \approx 10.5$ nT, and $B_{z\min} \approx -32.4$ nT. In the course of the magnetically quiet period, the Akasofu function

was smaller than 10 GJ/s, whereas two large peaks of up to 220 GJ/s and 160 GJ/s were observed to persist for 14 h

and 7 h, respectively, during 23 and 24 April 2023.

The magnitude of the background K_p index varied from 0 to 3, whereas it increased from 4 to 8.3 after 12:00 UT on

23 April 2023 and further decreased to 4. Yet another increase in the K_p index, up to 8, was observed between 03:00

UT and 06:00 UT on 24 April 2023. Before 08:00 UT on 23 April 2023, the magnitude of D_{st} varied from −30 nT to

5 nT. Over the interval ~18:00 UT on 23 April 2023 to ~01:00 UT on 24 April 2023, the D_{st} index showed a

minimum of about −170 nT, and it exhibited a new decrease of approximately −212 nT between ~01:00 UT and

~06:00 UT on 24 April 2023. After the latter, the D_{st} index increased from −212 nT to −25 nT. Thus, this storm is

the first in solar cycle 25 two-step severe geomagnetic storm with onset at 19:26 UT on 23 April 2023, which was

caused by a coronal mass ejection (Ghag et al., 2024).
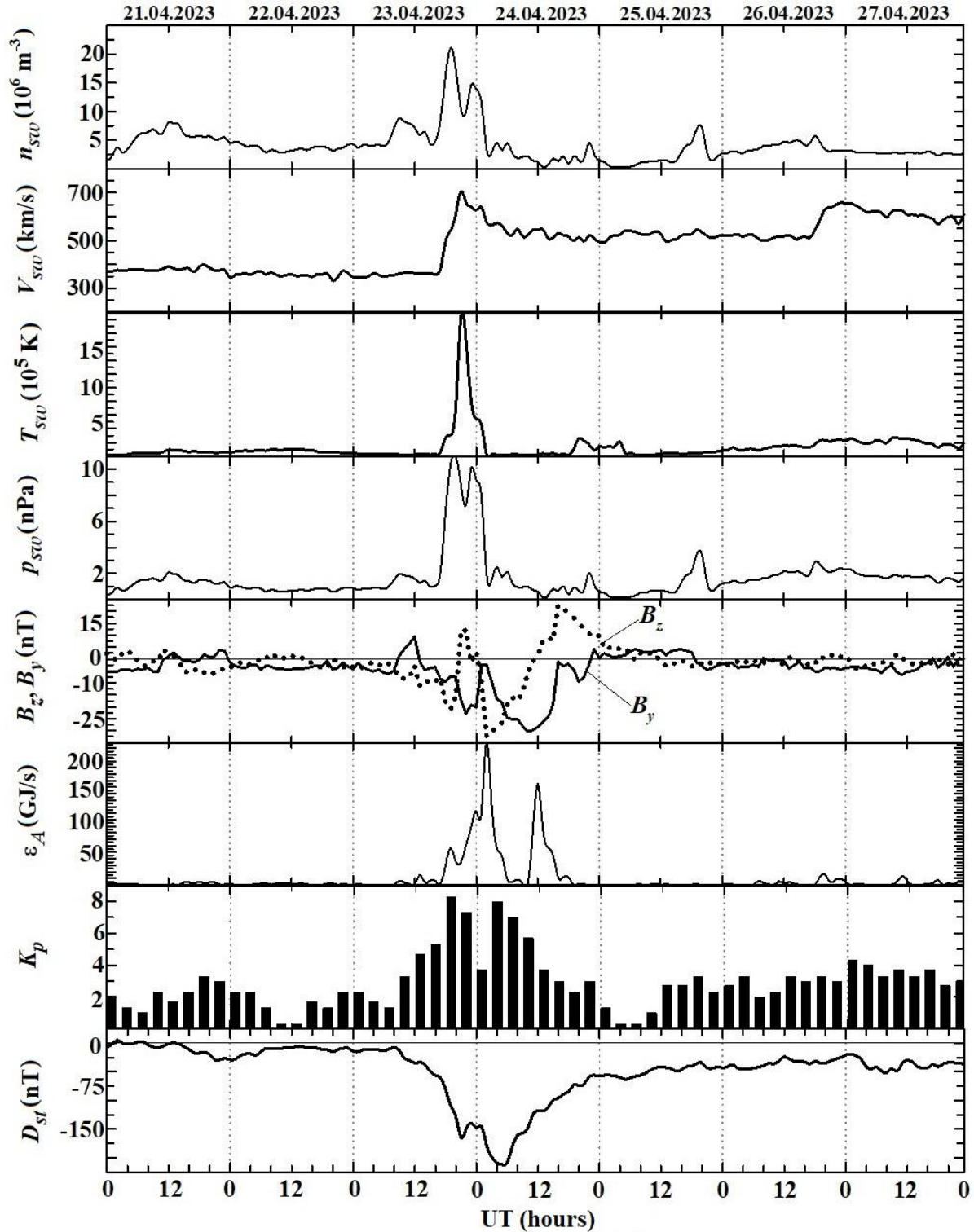
Figure 2: UT variations in the solar wind parameters: measured proton number density, n_{sw}, temperature, T_{sw}, plasma flow speed, V_{sw}, calculated dynamic pressure, p_{sw}, measured B_z and B_y components of the interplanetary magnetic field; variations of the calculated magnitude of the energy, ε_A, deposited into the Earth's magnetosphere from the solar wind per unit time; K_p- and D_{st} indices for the period April 21 – 27, 2023 (retrieved from **https://omniweb.gsfc.nasa.gov/form/dx1.html**; last access: 14 November 2023). Dates are indicated at the top of the figure.

173

208 strength was observed to increase by a factor of 2–10, attaining 100–200 nT at low-latitude stations and 300–700 nT
209 at high-latitude stations. Table 4 shows that the middle and low latitude stations in the eastern hemisphere recorded
210 geomagnetic field fluctuations generally not exceeding 10–20 nT on the quiet days, whereas the storm time
211 fluctuations exhibited an increase by a factor of 2–5, attaining 70–80 nT; however, at high latitude stations, the
212 fluctuations were close to 500–600 nT. As expected, the magnitude of variations in the geomagnetic field increased
213 with latitude, the variations in the strength of all component recorded at the stations nearly-equidistant from the
214 equator were close in value, and the geomagnetic field perturbations were also close in value at close latitudes in the
215 western and eastern hemispheres.
216

217 **Table 4** Peak-to-peak amplitude of the strength fluctuations in the geomagnetic field components recorded at the stations in the
218 eastern hemisphere.

Station	Background values (nT)			Disturbed values (nT)		
	X-component	Y-component	Z-component	X-component	Y-component	Z-component
PET	−10	−10	−4	−55	−77	−28
	+10	+10	+4	+70	+70	+29
KHB	−10	−10	−2	−50	−39	−14.5
	+10	+10	+2	+50	+54	+7.5
MMB	−10	−10	−2	−50	−35	−10
	+10	+10	+2	+47	+35	+12.5
KNY	−10	−8	−4	−35	−26	−20
	+10	+8	+4	+32	+28	+17
GUA	−8	−5	−2	−30	−19	−23
	+8	+5	+2	+70	+13	+12
KDU	−6	−7	−3	−42	−27	−8
	+6	+6	+3	+30	+21	+10
ASP	−10	−10	−2	−53	−44	−6.5
	+10	+8	+3	+39	+43	+12
CNB	−10	−10	−7	−62	−95	−28
	+10	+10	+8	+55	+64	+33
MCQ	−40	−40	−50	−530	−600	−320
	+70	+40	+50	+470	+340	+300
CSY	+50	+40	−50	−380	−180	−380
	−50	−40	+50	+160	+380	+290

219
220 The northward component of the geomagnetic field, X, usually showed the greatest perturbations in strength in both
221 hemispheres. The total durations of the disturbances were observed to be 26–30 hours. Thus, the geomagnetic storm,
222 the strongest in solar cycle 25, being a part of the geospace storm, established the state of space weather on a global
223 scale over 23–24 April 2023.
224
225 Geomagnetic field variations are produced by changing electric currents. Currents relevant to geomagnetic storms
226 comprise the magnetopause electric current flowing eastward near the equatorial plane, the westward current
227 through the magnetospheric tail and equatorial ring current within 3–6 earth radius from the Earth, and the
228 ionospheric currents in high latitude ionosphere.
229
230 During substorms, the electric current in the near tail can partially be diverted into the polar ionosphere along the
231 geomagnetic field lines closing the electric current through the substorm current wedge. As a result, the westward
232 equatorial electric current diminishes, which should be manifested by an increase in the horizontal component of the
233 geomagnetic field at the equator, and the westward ionospheric current increases at high latitudes, which is observed
234 as an increase in the horizontal intensity, H, of the geomagnetic field. The magnetic effect on the surface of the
235 Earth from the ionospheric currents significantly surpasses that from the tail current due to the proximity of the
236 ionosphere to the ground magnetometer stations.
237
238 As it happened, in the observations discussed in this paper, one of the two magnetometer chain was situated in the
239 night hemisphere of the Earth during both of the two steps of the 23–24 April 2023 geomagnetic storm. However,

240 the anticipated manifestations of the substorm current wedge can be easily seen only during the second step of the
241 23–24 April 2023 geomagnetic storm along the western hemisphere chain of magnetometer stations where the storm
242 was observed during night. The H components acquired at the equatorial latitude station TTB (geomagnetic latitude
243 7.15°N) and the high geomagnetic latitude OTT (geomagnetic latitude 54.28°N) station are shown in the top panel
244 of Fig. 3. Just before 04:00 UT, a partial diversion of the ring or tail current into the ionosphere through field-
245 aligned currents occurred and yielded an increase in the intensity of the horizontal intensity, H, of the geomagnetic
246 field at the TTB station and a simultaneous decrease in H at high latitude OTT station. In the southern hemisphere,
247 the northern component is also positive (Kepko et al., 2015), as can be seen in the magnetogram acquired at AIA
248 station (Fig. 3, bottom panel).
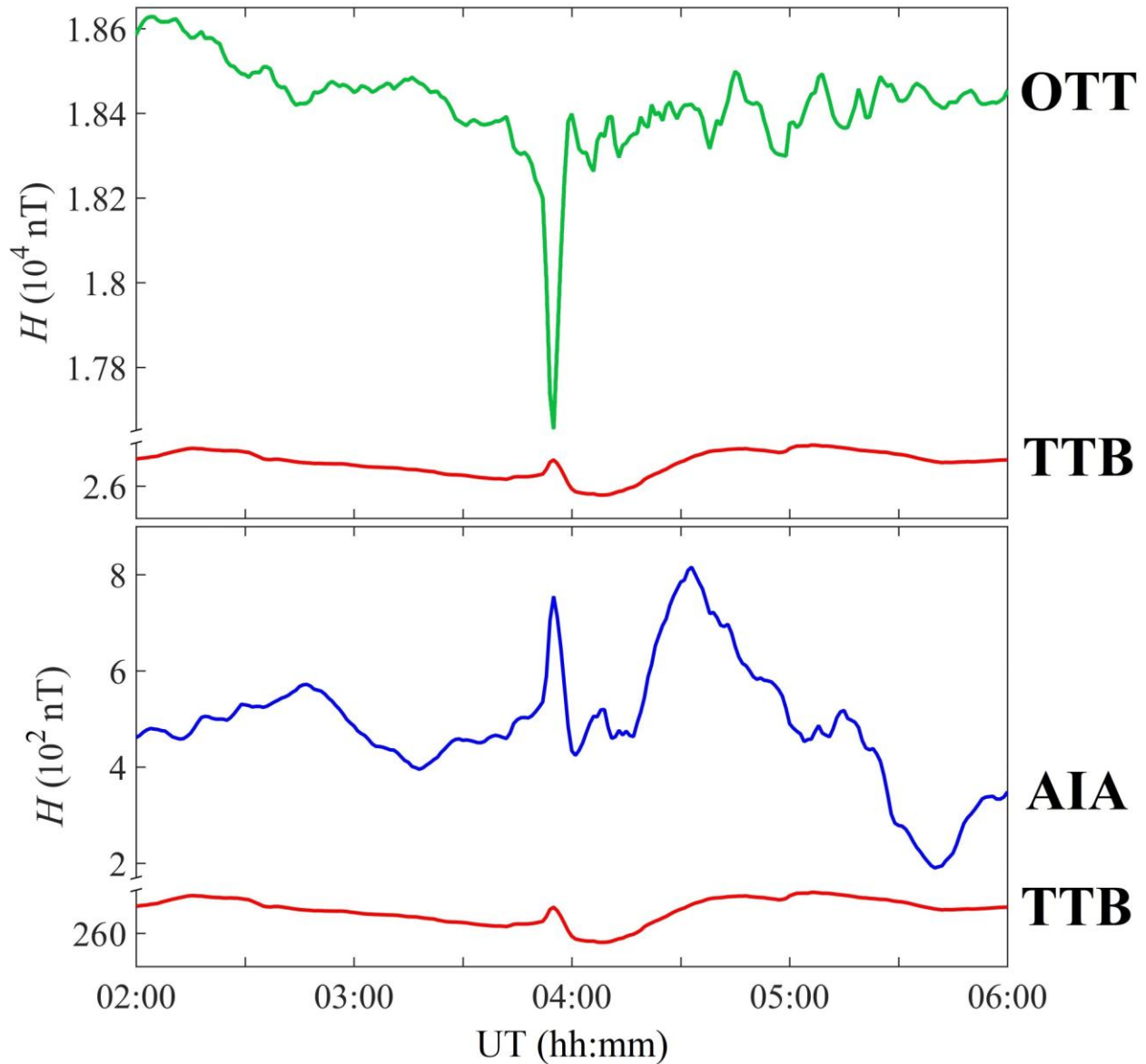
249
250 **Figure 3: Magnetograms from high latitude OTT and AIA stations and equatorial TTB station on the night side during**
251 **the second step of the 23–24 April 2023 geomagnetic storm.**

252 Processes analogous to those reported above are not observed during the first step of the 23–24 April 2023
253 geomagnetic storm along the eastern hemisphere chain of magnetometer stations where the first step of the storm
254 was observed during night. As was described in the Introduction section, the strength of the interplanetary magnetic
255 field B_z component attained ~ −22 nT during the first step and ~ −30 nT during the second step of the severe
256 geomagnetic storm (Ghag et al., 2024,). Thus, these observations indicate that there is a B_z threshold for diverting

257 the cross-tail current through the current wedge into the ionosphere. For the 23–24 April 2023 geomagnetic storm, a
258 threshold value lies between −22 nT and −30 nT.
259
260 Generally, the diversion of cross-tail current into the ionosphere is dependent on initial conditions, precondition, and
261 memory, or complexity, of the magnetosphere-ionosphere system (CEDAR: The New Dimension,
262 https://cedarscience.org/sites/default/files/2021-10/CEDAR_October_V9.2.pdf). Since the state of the
263 magnetosphere system continuously evolves, and therefore, the data on one-step geospace storms occurring
264 separately are not suitable for comparison. To make the influence of such uncertainties minimal, the need to deal
265 with two storms occurring as close as possible to each other arises, which makes a two-step geospace storm a solar-
266 terrestrial event of opportunity for realizing a technique for estimating the IMF B_z threshold for the formation of the
267 substorm current wedge.
268
269 The future studies on this topic is no doubt needed to confirm our conclusions, and they include the validation of
270 features discovered in this study, the determination of thresholds for other storms, and modeling the formation of the
271 current wedge.
272
273 The results obtained are of importance for both achieving the fundamental physical understanding and a quantitative
274 assessment of energy storage in the ionosphere-magnetosphere system and its release via a partial diversion of the
275 ring or tail current into the ionosphere through field-aligned currents (CEDAR: The New Dimension,
276 https://cedarscience.org/sites/default/files/2021-10/CEDAR_October_V9.2.pdf , last access October 15, 2024,
277 2010). The ionospheric perturbations produced by the energy release can also be of importance to radio
278 communications, including HF radio communications (Wang et al., 2022; Wang et al., 2023).

5 Conclusions

280 The intercomparisons of the geomagnetic field variations recorded at two near meridional chains of magnetometer
281 stations in the western and eastern hemispheres yield the following results:
282
283 1. Part of the near-Earth cross-tail current closed itself via the ionosphere, to which it was linked by the substorm
284 current wedge, and manifested itself in the magnetograms acquired at equatorial and high latitude stations on the
285 night side of the Earth.
286
287 2. This study identifies, for the first time, that the emergence of a current wedge may be quantified by a threshold
288 value of the interplanetary magnetic field (IMF) B_z component utilizing observations made during a two-step
289 geospace storm with ground-based magnetometers.
290
291 3. The two-step character of this storm has allowed author to identify that the B_z interplanetary magnetic field
292 component threshold for the formation of the substorm current wedge lies within the –(22–30) nT interval.
293
294 4. The study, for the first time, convincingly attest to the two-step geospace storm to be an ideal solar-terrestrial
295 event of opportunity for realizing a technique for estimating the IMF B_z component threshold for the formation of
296 the substorm current wedge.
297
298 4. Under quiet conditions, the geomagnetic field components usually exhibited variations not exceeding 40–50 nT in
299 the western hemisphere and 10–20 nT in the eastern hemisphere.
300
301 5. During the severe geomagnetic disturbance of 23–24 April 2023, the strength fluctuations increased by a factor of
302 2–10 and 2–5 in the western and eastern hemispheres, respectively, attaining 300–700 nT.
303
304 6. The northward component of the geomagnetic field, X, was observed to be most disturbed in the western and
305 eastern hemispheres. The total durations of the disturbances were observed to be 26–30 hours.
306
307 7. The geomagnetic field components showed variations in the strength increasing with latitude. The strength
308 fluctuations recorded at the stations nearly-equidistant from the equator were close in value. This is true for both the
309 western and eastern hemispheres.

310
311   8. Also close in value were the perturbations in the strength recorded at the stations at close latitudes but in different
312   hemispheres.
313
314   9. The first two-step severe geomagnetic storm in solar cycle 25 to date, as a component of the geospace storm,
315   significantly affected the state of space weather on a global scale on 23–24 April 2023.
316

Appendix

Analysis of magnetometer data

Analysis of temporal variations in the relative strength of the northward X-, eastward Y-, and vertical Z-component of the geomagnetic field over the period 20–26 April 2023 has been performed. The geospace storm occurred within the period 23–24 April 2023, the data for which are shown against the background of a quiet time noise recorded during 20–22 and 25–26 April 2023.

A.1 Western hemisphere

GDH Station. From 00:00 UT to 10:00 UT over the geomagnetically quiet interval 20–22, 25, and 26 April 2023, the strength of the northward component of the geomagnetic field, X, showed fluctuations within ±50 nT (Fig. A.1), while between 10:00 UT and 18:00 UT the strength fluctuations increased to 60–145 nT with the energy spectrum almost flat. On 23 April 2023, the variations in the X-component developed into non-monotonous and even quasi-periodic changes between 10:00 UT and 24:00 UT, when the X-component strength varied from 120 nT to 180 nT. Considerable disturbances, up to –550 nT, took place at around 11:15 UT on 24 April 2023, and only after 16:00 UT on 24 April 2023 the level of fluctuations approached ±50 nT. The recovery phase persisted for 25 and 26 April 2023.

Between 00:00 UT and 10:00 UT on 20–23 and 25, 26 April 2023, the variations in the eastward component of the geomagnetic field, Y, were relatively insignificant, up to 50 nT, while between 10:00 UT and 18:00 UT, they were observed to reach up to ±100 nT. The variations in the Y-component showed non-monotonousness and, at times, quasi-periodicity over a span of 14 hours from 10:00 UT to 24:00 UT on 23 April 2023, with a drop in the strength down to –220 nT after 19:30 UT. From 11:00 UT to 12:00 UT on 24 April 2023, the strength varied from 340 nT to –300 nT.

On 20–23 and 25, 26 April 2023, the variations in the vertical component of the geomagnetic field, Z, strength were quite smooth, within ±100 nT from 00:00 UT to 08:00 UT, while after 10:00 UT and towards the end of the day, the variations enhanced, with peak-to-peak amplitude attaining 340 nT. Between 00:00 UT and 14:00 UT on 23 April 2023, the Z-component showed significant fluctuations in strength, with peak-to-peak amplitude of 150 nT and a maximum of 100 nT. During the period 12:00 UT on 23 April 2023 to 14:00 UT on 24 April 2023, the strength variations exhibited non-monotonousness and, at times, quasi-periodicity. At about 20:00 UT on 23 April 2023, the strength reached –230 nT. After 09:00 UT on 24 April 2023, the strength varied from 380 nT to –430 nT, which was recorded between about 11:00 UT and 12:00 UT.

GDH Greenland

OTT Canada
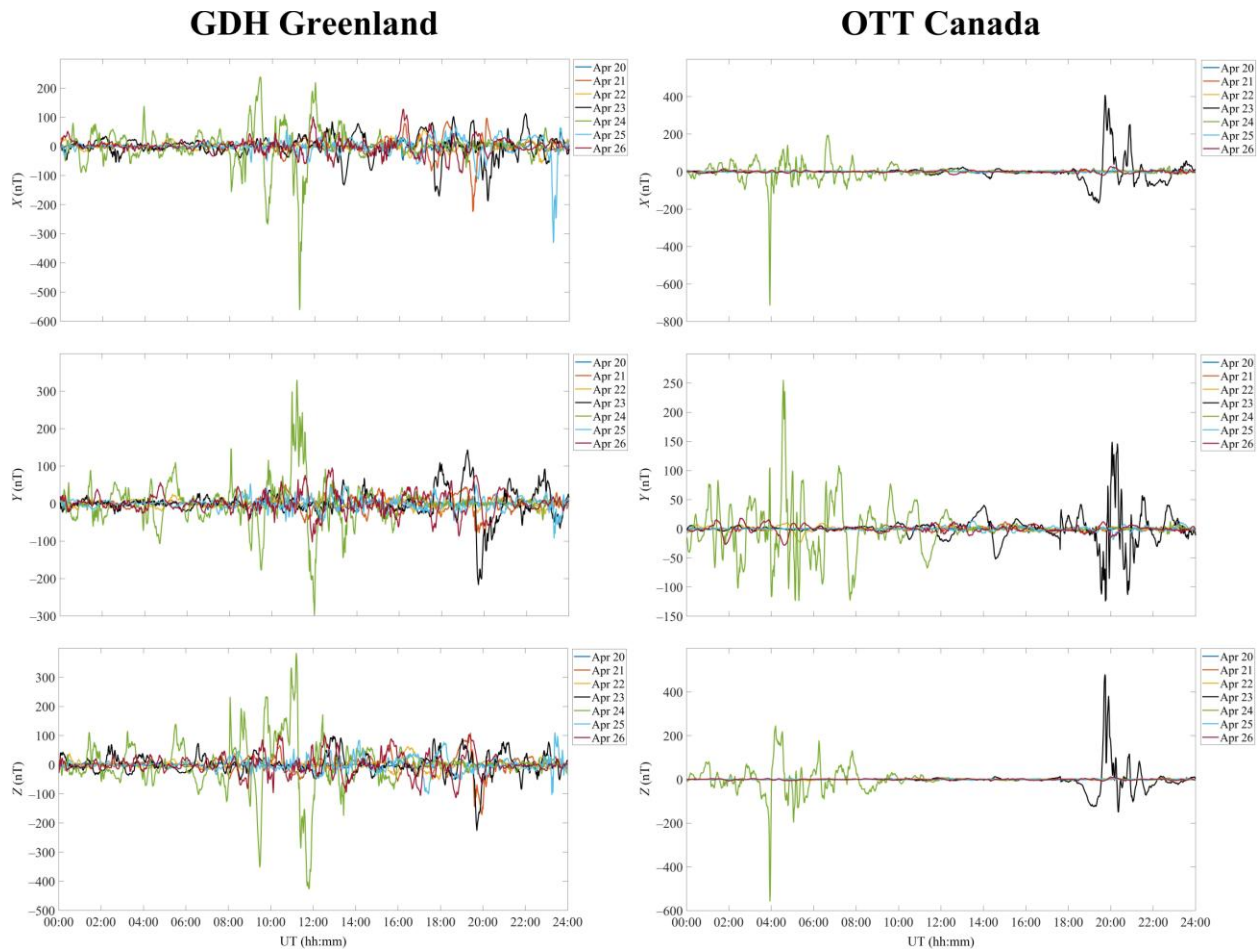
353
354 **Figure A.1: UT variations of the geomagnetic field at the GDH station (geographic coordinates 69.2520°N, 53.5330°W,**
355 **geomagnetic coordinates 77.52°N, 32.69°E) and at the OTT station (geographic coordinates 45.4030°N, 75.552°W,**
356 **geomagnetic coordinates 54.46°N, 3.51°W) over the period 20–26 April 2023.**

357
358 *OTT Station*. On the days used as a quiet time reference period, the variations in the strength of the northward
359 component of the geomagnetic field, *X*, rarely exceeded ±20 nT (Fig. A.1). On 23 April 2023, sharp increases of up
360 to 250–420 nT in the strength of the *X*-component were observed from 19:30 UT to 22:00 UT; and from 21:00 UT
361 to 22:30 UT, the *X*-component strength decreased approximately to −100 nT. Between 03:00 UT and 09:30 UT on
362 24 April 2023, the magnetic field strength fluctuated mainly from −100 nT to 200 nT, and only at 03:55 UT, it
363 briefly dropped to −710 nT. Immediately after 14:00 UT on 24 April 2023, the variations in the *X*-component
364 strength became smaller than a few tens of nT.

365
366 Monotonous variations in the eastward component of the geomagnetic field, *Y*, strength did not exceed ±30 nT
367 during geomagnetically quiet times, whereas over the period 10:00 UT on 23 April 2023 to 13:00 UT on 24 April
368 2023, the *Y*-component exhibited large fluctuations in strength, from −125 nT to 257 nT.

369
370 During magnetically quiet times, the vertical component of the geomagnetic field, *Z*, strength showed quite smooth
371 variations, the amplitude of which was smaller than a few tens of nT. During the period 19:00 UT on 23 April 2023
372 to 10:00 UT on 24 April 2023, the *Z*-component fluctuated wildly, first from −140 nT to 490 nT near 19:40 UT on
373 23 April 2023, then within ±80 nT after 00:00 UT, and then it decreased to −560 nT at around 03:55 UT on 24 April
374 2023.

375
376 *FRD Station*. The variations in the northward component of the geomagnetic field, *X*, did not exceed 10–15 nT
377 during magnetically quiet times (Fig. A.2), while between about 10:00 UT on 23 April 2023 and 12:00 UT on 24
378 April 2023, its variations showed non-monotonousness, and an increase in *X*- component strength that occurred over

379 the interval 19:45–23:35 UT. The X-component exhibited fluctuations within –52–67 nT on 24 April 2023, with a
380 minimum of –76 nT at about 04:10 UT; after about 12:00 UT, significant variations ceased.
381
382 During magnetically quiet times, the variations in the eastward component of the geomagnetic field, Y, strength were
383 smaller than ±20 nT, including the disturbance-daily variation. During a period from 10:00 UT on 23 April 2023 to
384 13:00 UT on 24 April 2023, the strength fluctuations were large, with a minimum of –70 nT that occurred between
385 19:30–21:00 UT on 23 April 2023. An increase in the strength within –60–115 nT was observed to occur between
386 02:00 UT and 12:00 UT on 24 April 2023.
387
388 Over a span of magnetically quiet times, the vertical component of the geomagnetic field, Z, strength, weakly
389 fluctuating, changed its magnitude by less than 5 nT. The noticeable variations in its magnitude began at around
390 14:00 UT on 23 April 2023 and ended at about 12:00 UT on 24 April 2023, with maximums of ~44 nT observed at
391 around 20:00 UT and 21:00 UT on 23 April 2023, and a minimum of –39 nT at about 04:00 UT on 24 April 2023.
392
393 *SJG Station*. During magnetically quiet times, the fluctuations in strength of the northward component of the
394 geomagnetic field, X, were smaller than ±7 nT (Fig. A.2). The noticeable variations in strength began at around
395 11:00 UT on 23 April 2023 and were over past 14:00 UT on 24 April 2023, with minimums of about –28 nT at
396 approximately 20:50 UT on 23 April 2023 and of about –42 nT at around 04:10 UT on 24 April 2023, and with
397 maximums of 30 nT at about 01:30 UT and 05:00 UT on 24 April 2023.
398
399 The eastward component of the geomagnetic field, Y, strength showed insignificant variations, ~7 nT, before 10:00
400 UT on 20–23 and 25, 26 April 2023, while between 10:00 UT on 23 April 2023 and 14:00 UT on 24 April 2023, the
401 Y-component strength exhibited non-monotonous and significant disturbances, with a minimum of about –35 nT at
402 19:40 UT on 23 April 2023 and a maximum of about 26 nT at 07:15 UT on 24 April 2023.
403
404 During magnetically quiet times, the vertical component of the geomagnetic field, Z, strength showed variations
405 smaller than ±3 nT. The non-monotonous and significant fluctuations in the strength of this component were
406 observed to occur starting at 12:00 UT on 23 April 2023 and ending at 14:00 UT on 24 April 2023, with a minimum
407 of about –11.5 nT and a maximum of about 11.5 nT.
408

FRD USA   **SJG USA**
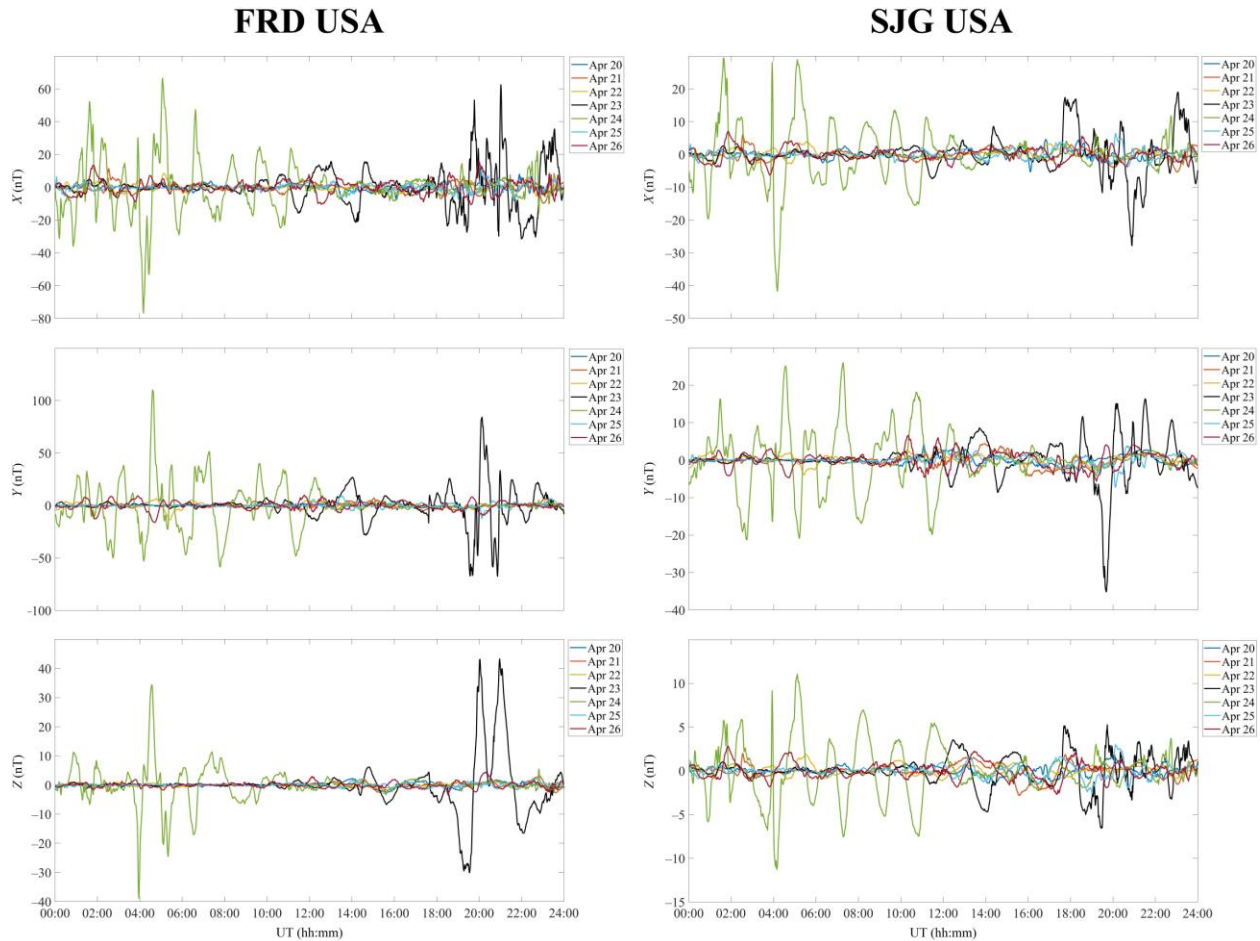
409
410 **Figure A.2: UT variations of the geomagnetic field at the FRD station (geographic coordinates 38.2100°N, 77.3670°W,**
411 **geomagnetic coordinates 47.25°N, 5.47°W) and at the SJG station (geographic coordinates 18.1100°N, 66.1500°W,**
412 **geomagnetic coordinates 27.20°N, 6.96°E) over the period 20–26 April 2023.**

413 *KOU Station*. During magnetically quiet times, as well as until 14:00 UT on 23 April 2023, the variations in the
414 strength of the northward component of the geomagnetic field, X, were smaller than ±10 nT (Fig. A.3). Over the
415 period 11:00 UT on 23 April 2023 to 16:00 UT on 24 April 2023, the X-component showed significant
416 enhancements in its variations that become non-monotonous, with a maximum of 35 nT at 21:00 UT on 23 April
417 2023 and a minimum of −53 nT at 04:10 UT on 24 April 2023.
418
419 During the quiet time reference period, the eastward component of the geomagnetic field, Y, exhibited variations
420 attaining ±8 nT, whereas its strength considerably decreased, to −27 nT, at 19:40 UT on 23 April 2023, after which
421 it increased to 52 nT at 21:30 UT. Between 00:00 UT and 12:00 UT on 24 April 2023, the Y-component showed
422 large non-monotonous fluctuations in strength attaining ±25 nT.
423
424 The vertical component of the geomagnetic field, Z, showed strength fluctuations usually smaller than ±(5–7) nT,
425 while significant time variations in strength persisted for the period 10:00 UT on 23 April to 16:00 UT on 24 April
426 2023, with a minimum of about −22.5 nT at around 14:20 UT on 23 April 2023 and a maximum of ~18 nT at
427 approximately 19:30 UT on the same day. During the course of the day 24 April 2023, the Z-component exhibited
428 variations within −21nT to 19 nT.
429

KOU France   **TTB Brazil**

430
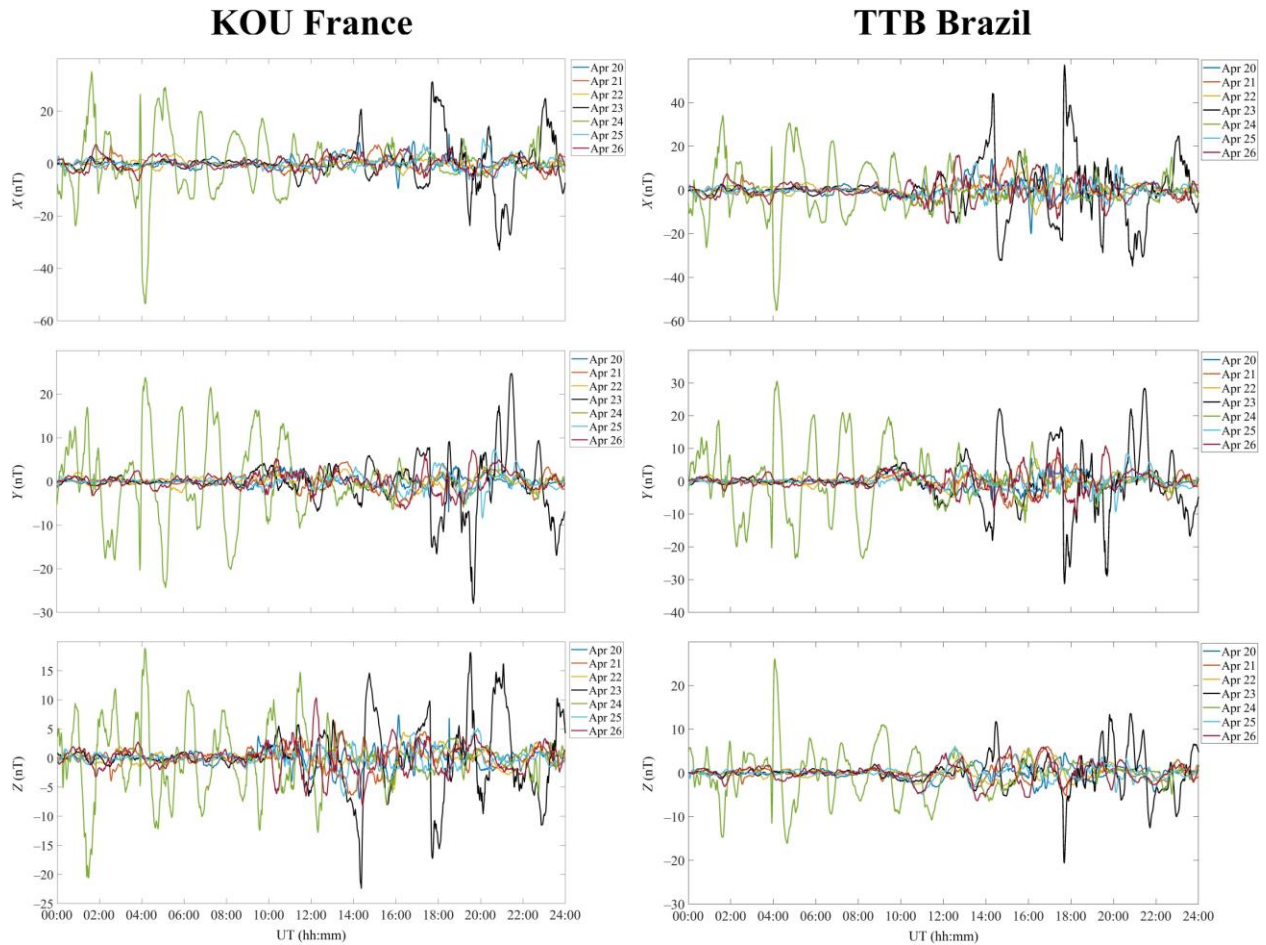
Figure A.3: UT variations of the geomagnetic field at the KOU station (geographic coordinates 5.2100°N, 52.730°W, geomagnetic coordinates 13.87°N, 20.46°E) and at the TTB station (geographic coordinates 1.2050°S, 48.5130°W, geomagnetic coordinates 7.25°N, 24.35°E) over the period 20–26 April 2023.

TTB Station. On quiet time reference days, the northward component of the geomagnetic field, *X*, showed variations smaller than ±20 nT (Fig. A.3), which developed into non-monotonous and significant variations over a span of time between ~10:00 UT on 23 April 2023 and ~16:00 UT on 24 April 2023. The field strength had minimums of −35 nT and −55 nT at ~21:00 UT on 23 April 2023 and at 04:10 UT on 24 April 2023, respectively, and a maximum of 57 nT at 17:40 UT on 23 April 2023.

The quiet time eastward component of the geomagnetic field, *Y*, strength usually exhibited variations smaller than ±10 nT, whereas on 23 April 2023 a minimum strength of −31 nT was recorded at ~17:45 UT and a maximum of about 29 nT at 21:35 UT on 23 April 2023. The significant variations in the *Y*-component persisted through to 18:00 UT on 24 April 2023, with a maximum of 30 nT at 04:10 UT on 24 April 2023.

During magnetically quiet times, the vertical component of the geomagnetic field, *Z*, exhibited variations within ±7 nT. Approximately from 12:00 UT on 23 April 2023 to 19:00 UT on 24 April 2023, this component showed fluctuations in strength from−20 nT to 26 nT.

PIL Station. On quiet time reference days, the northward component of the geomagnetic field, *X*, exhibited strength variability within ±10 nT (Fig. A.4), while it showed a significant increase in non-monotonous variations over the interval 11:00 UT on 23 April 2023 to 14:00 UT on 24 April 2023. The positive spikes of 37 nT and 47 nT were observed to occur at 17:40 UT on 23 April 2023 and at ~04:00 UT on 24 April 2023, respectively, while the negative spikes of −47 nT and −68 nT to occur at 21:00 UT on 23 April 2023 and at 04:10 UT on 24 April 2023, respectively.

456
457   The eastward component of the geomagnetic field, *Y*, strength showed variability within a few nT under quiet time
458 conditions, while from 12:00 UT on 23 April 2023 to 16:00 UT on 24 April 2023 this component variations became
459 non-monotonous and significant, with spike strengths attaining 6.5 nT and alternating decrease strengths reaching −7
460 nT over the interval 19:00 UT to 20:00 UT on 23 April 2023, and a drop of −10.5 nT at approximately 04:40 UT on
461 24 April 2023.
462
463   During magnetically quiet times, the vertical component of the geomagnetic field, *Z*, showed variations smaller than
464 a few nT, whereas it exhibited considerable and sharp variations from 10:00 UT on 23 April 2023 to 16:00 UT on 24
465 April 2023. The *Z*-component strength fell to −7.3 nT at approximately 04:10 UT on 24 April 2023, while its
466 magnitude was close to 3 nT at about 16:00 UT.
467
468   *AIA Station*. On quiet time reference days, the northward component of the geomagnetic field, *X*, exhibited strengths
469 rarely exceeding ±20 nT (Fig. A.4). Considerable and sharp variations in this component strength began at around
470 18:00 UT on 23 April 2023 and continued until 12:00 UT on 24 April 2023. During 23 April 2023, the *X*-component
471 strength was observed to vary from −100 nT to 290 nT, while it showed greater variability on 24 April 2023 when
472 the strength varied from −380 nT to 200 nT.
473
474   The quiet time eastward component of the geomagnetic field, *Y*, strength showed variability within ±30 nT. The
475 significant and sharp variations in the *Y*-component began at 13:00 UT on 23 April 2023 and persisted for 24 h. On
476 23 April 2023, the *Y*-component showed strength fluctuations from −230 nT to 150 nT, which increased from −400
477 nT to 240 nT on 24 April 2023.
478
479   Under quiet time conditions, the vertical component of the geomagnetic field, *Z*, exhibited fluctuations in strength
480 smaller than ±20 nT. From 18:00 UT on 23 April 2023 to 13:00 UT on 24 April 2023, the strength variations were
481 sharp and significant. The *Z*-component showed strength variations within −250–170 nT on 23 April 2023, and
482 within −215–300 nT on 24 April 2023.
483
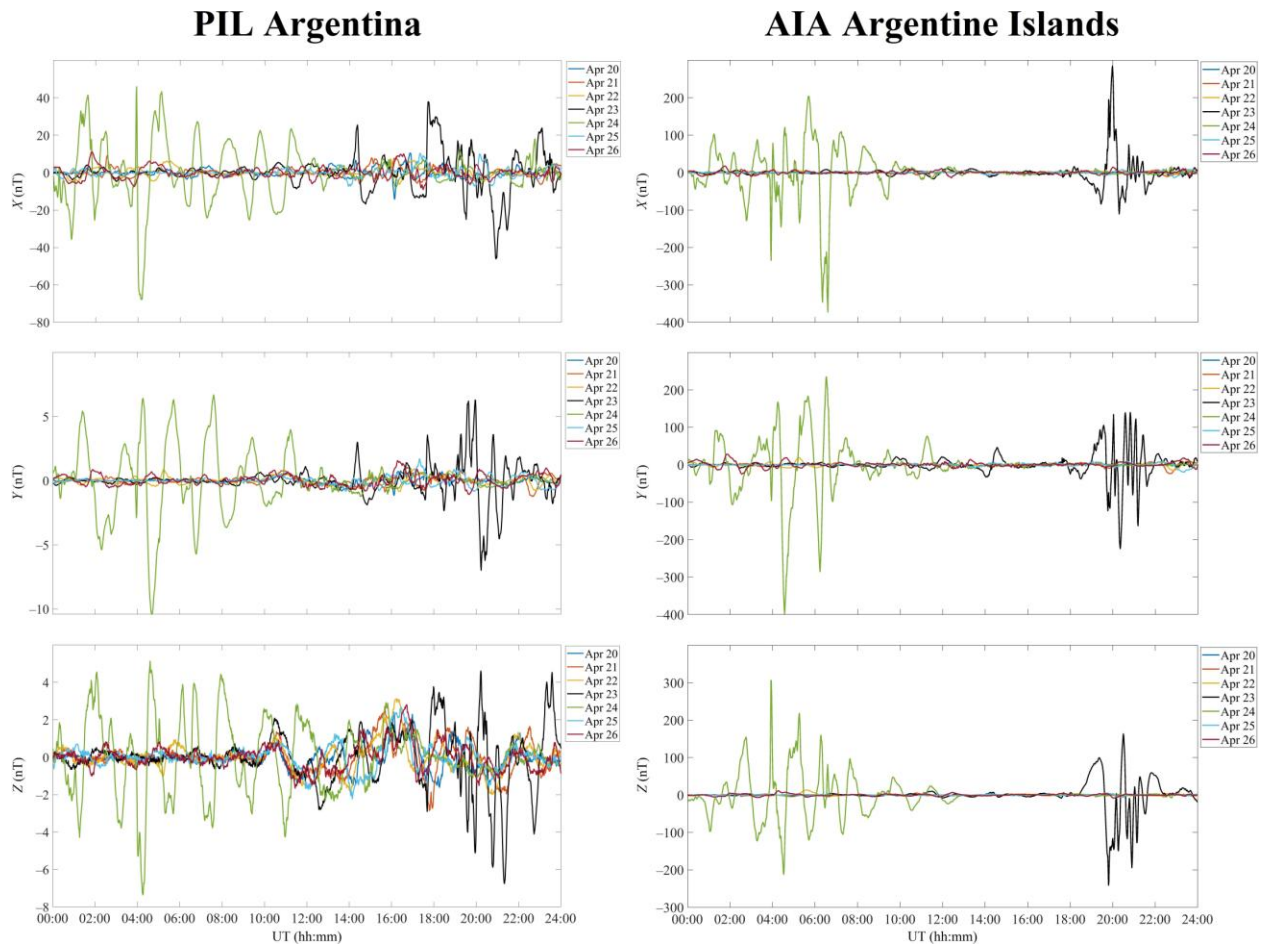
Figure A.4: UT variations of the geomagnetic field at the PIL station (geographic coordinates 31.6670°S, 63.881°W, geomagnetic coordinates 22.33°S, 8.08°E) and at the AIA station (geographic coordinates 65.2450°S, 64.2580°W, geomagnetic coordinates −55.91°, +6.30°) over the period 20–26 April 2023.

A.2. Eastern Hemisphere

PET Station. On quiet time reference days, the northward component of the geomagnetic field, *X*, exhibited moderate variability within ±10 nT (Fig. A.5). Considerable and sharp strength variations began after 10:30 UT on 23 April 2023 and persisted past 11:30 UT on 24 April 2023, with the strength fluctuating within −55 nT–43 nT on 23 April 2023, and from −45 nT to 70 nT on 24 April 2023.

The quiet time eastward component of the geomagnetic field, *Y*, strength variations were smaller than ±15 nT. The amplitude fluctuations considerably increased past 10:00 UT on 23 April 2023 and persisted until 12:00 UT on 24 April 2023. In the course of the first day, the amplitude fluctuations in strength occurred within −77 nT to 70 nT, while they occurred around a lower strength level, from −57 nT to 50 nT, on the second day.

During the quiet time reference period, the vertical component of the geomagnetic field, *Z*, showed fluctuations in strength with amplitudes varying from about −7 nT to 6 nT. The fluctuations notably increased after 10:00 UT on 23 April 2023 and continued until 13:00 UT on 24 April 2023. On 23 April 2023, the *Z*-component exhibited variations in strength from −28 nT to 18 nT, while it showed variations from −15 nT to 29 nT the next day.
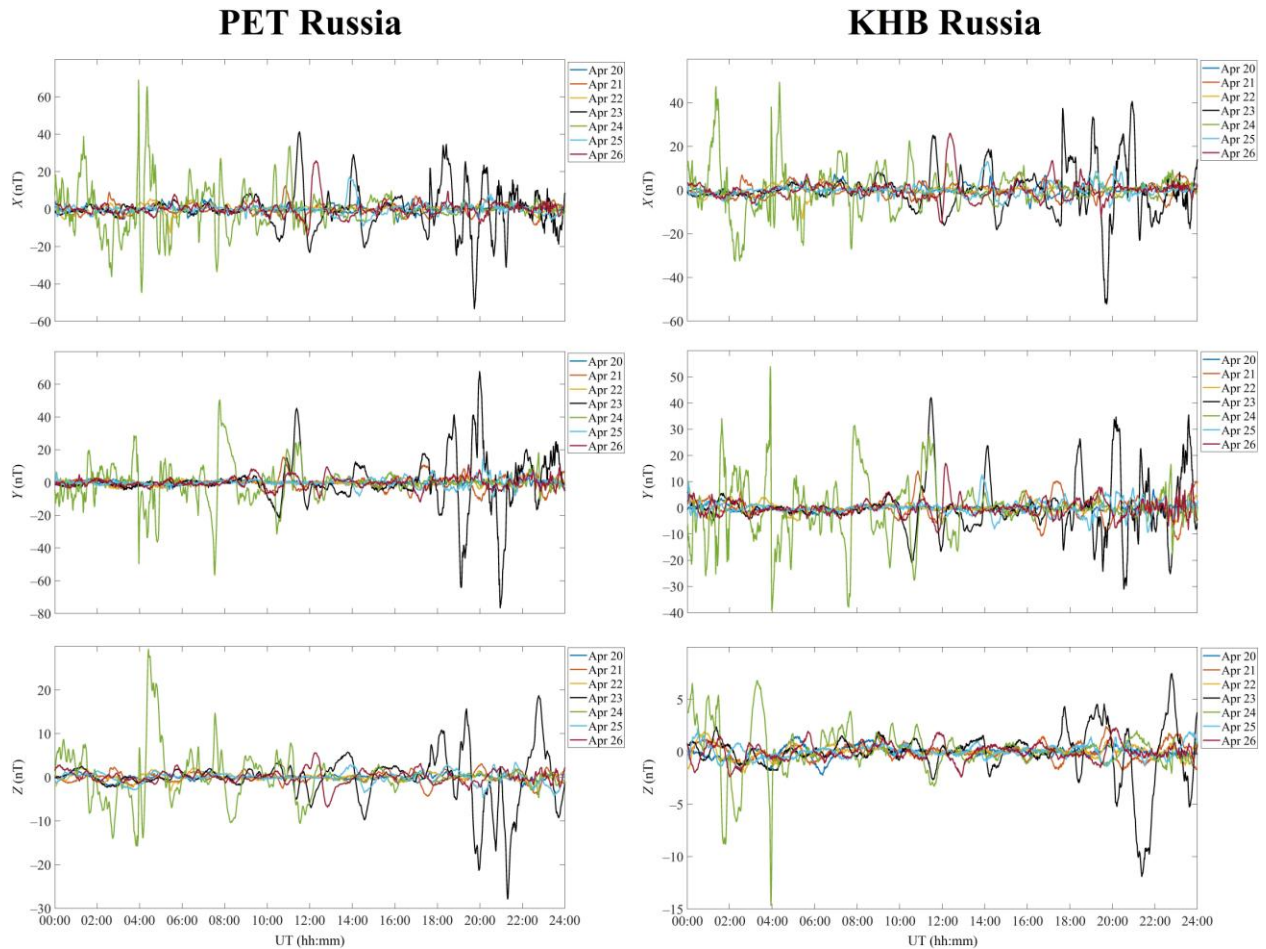
Figure A.5: UT variations of the geomagnetic field at the PET station (geographic coordinates 52.9710°N, 158.2480°E, geomagnetic coordinates +46.63, +222.93) and at the KHB station (geographic coordinates 47.61°N, 134.68°E, geomagnetic coordinates 39.05°N, 156.42°W) over the period 20–26 April 2023.

KHB Station. On quiet time reference days, the northward component of the geomagnetic field, *X*, strength showed variations generally not exceeding ±10 nT (Fig. A.5). The pronounced enhancements in sharp variations of the *X*-component strength began after about 11:00 UT on 23 April 2023 and continued until 16:00 UT on 24 April 2023. On 23 April 2023, the *X*-component strength exhibited variations within −50 nT to 40 nT, and it showed variations from −30 nT to 50 nT on 24 April 2023.

The quiet time eastward component of the geomagnetic field, *Y*, variations were observed to occur mainly within ±10 nT, rarely attaining 20 nT. The amplitude fluctuations showed a noticeable increase after 10:00 UT on 23 April 2023, with the disturbance continuing through to 14:00 UT on 24 April 2023. On the first day, the *Y*-component showed fluctuations from −30 nT to 43 nT, and on the second day within −39 nT to 54 nT.

The vertical component of the geomagnetic field, *Z*, exhibited insignificant temporal variability within ±2 nT on the days used as a quiet time reference period, whereas the strength was observed to increase to 7.5–12 nT on 23 April 2023. On 24 April 2023, the component showed strength fluctuations within −14.5 nT to 7 nT. In total, the enhanced fluctuations persisted for about 26 h.

MMB Station. The strengths of the northward component of the geomagnetic field, *X*, showed quiet time variations generally smaller than ±20 nT, but most frequently they were confined to ±10 nT (Fig. A.6). Enhanced variations in the *X*-component strength began before 10:00 UT on 23 April 2023 and continued through to 12:00 UT on 24 April 2023, with the strength of this component changing from −50 nT to 40–47 nT.

532   The quiet time variations in the eastward component of the geomagnetic field, Y, strength reached ±10 nT.
533   Significant variations in the Y-component strength began at about 10:00 UT on 23 April 2023 and continued through
534   to about 13:00 UT on 24 April 2023, with the variations in this component strength not exceeding ±35 nT on the
535   first day, and showing temporal variability within ±(30–35) nT on the second day.
536
537   On the days used as a quiet time reference period, the vertical component of the geomagnetic field, Z, strength
538   exhibited temporal variability within a few nT, whereas they noticeably increased at ~10:00 UT on 23 April 2023
539   and persisted until 13:00 UT on 24 April 2023, with fluctuations attaining ±(10–12.5) nT.
540
541   *KNY Station*. The northward component of the geomagnetic field, X, generally exhibited variations in strength
542   smaller than ±10 nT (Fig. A.6). The strength fluctuations showed a sharp increase after 10:00 UT on 23 April 2023
543   and continued to 16:00 UT on 24 April 2023. On 23 April 2023, the strength exhibited variations within −35 nT to
544   31 nT, and within −28 nT to 32 nT the following day.
545
546   The quiet time variations in the eastward component of the geomagnetic field, Y, strength occurred within ±8 nT.
547   After 10:30 UT on 23 April 2023, the strength fluctuations increased from −12 nT to 28 nT. The next day, this
548   component strength exhibited temporal variability within −26 nT to 27 nT.
549
550   On the quiet time reference days, the vertical component of the geomagnetic field, Z, showed variations in strength
551   from −6 nT to 11 nT. The strength variations exhibited a noticeable increase after 10:00 UT on 23 April 2023 and
552   continued through to about 16:00 UT on 24 April 2023, with the fluctuations within ±20 nT.
553
554   *GUA Station*. The quiet time variations in the northward component of the geomagnetic field, X, generally did not
555   exceed 7–8 nT (Fig. A.7). Enhanced strength fluctuations were observed to occur over the interval 10:00 UT on 23
556   April 2023 to 06:00 UT on 24 April 2023. On 23 and 24 April 2023, the strength of this component varied from −30
557   nT to 47 nT, occasionally to 70 nT.
558
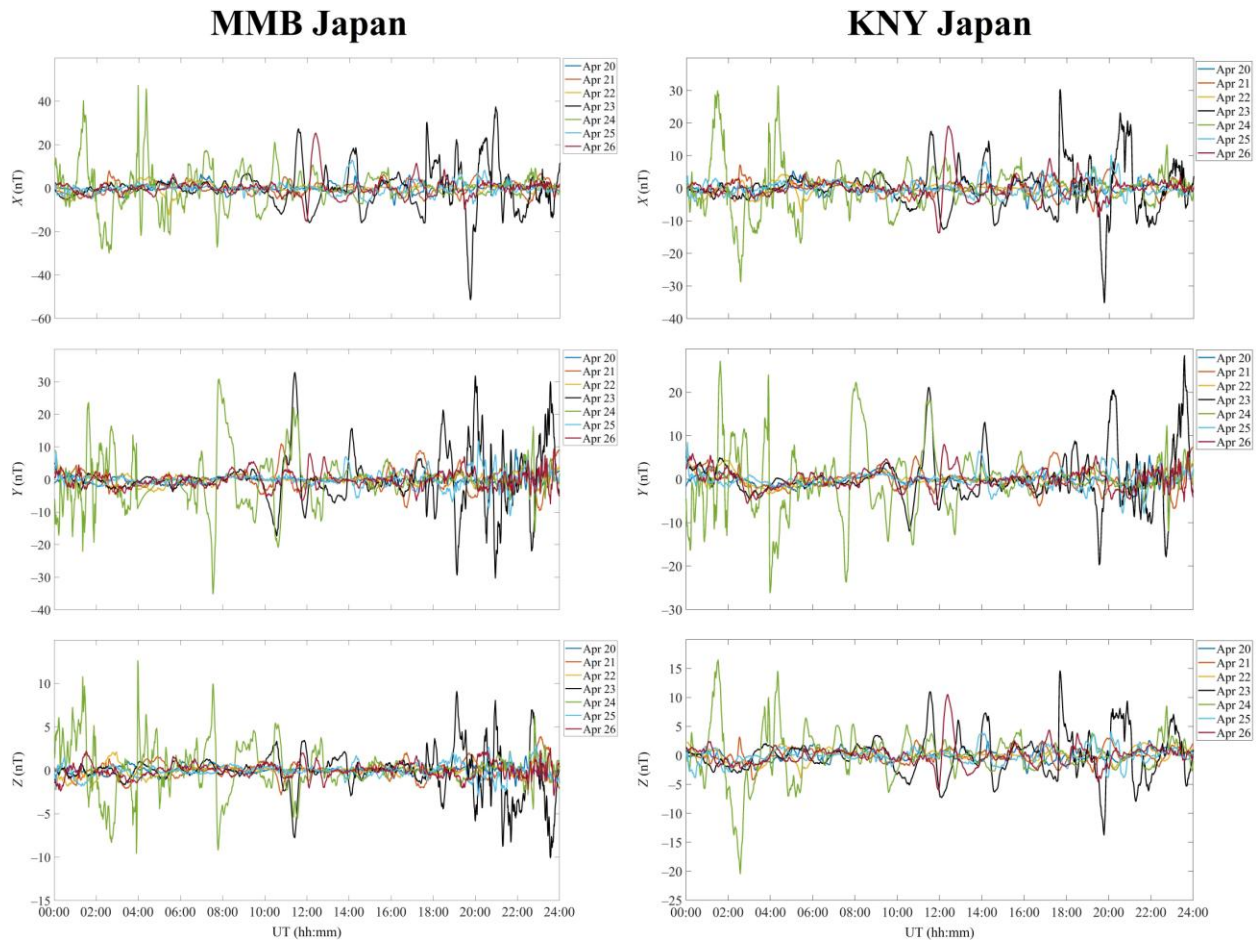
Figure A.6: UT variations of the geomagnetic field at the MMB station (geographic coordinates 43.91°N, 144.19°E, geomagnetic coordinates 36.09°N, 147.57°W) and at the KNY station (geographic coordinates 31.42°N, 130.88°E, geomagnetic coordinates 22.70°N, 158.28°W) over the period 20–26 April 2023.

The eastward component of the geomagnetic field, Y, exhibited fluctuations in strength within ±5 nT on the days used as a quiet time reference period. Enhancements in the strength fluctuations occurred over the interval 10:00 UT on 23 April 2023 to 14:00 UT on 24 April 2023. On the first day, the strength of this component varied from −8 nT to 12 nT, and on the second day it varied within −12 nT to 13 nT. A brief ~19-nT drop in the strength of this component was seen at around 04:00 UT on 24 April 2023.

The vertical component generally exhibited variations in the strength smaller than a few nT. Noticeable increases in the variations of the strength of this component were observed to occur over the interval 10:00 UT on 23 April 2023 to 05:00 UT on 24 April 2023. On 23 April 2023, the Z-component strength fluctuations occurred within ±7 nT, while the following day they exhibited variations within −10 nT to 12 nT, with a brief decrease by 23 nT at about 04:00 UT.

KDU Station. On the days used as a quiet time reference period, the variations in the strength of the northward component of the geomagnetic field, X, were observed to occur within ±6 nT (Fig. A.7). On 23 April 2023, the fluctuations in strength occurred within −42 nT to 28 nT from 10:00 UT to 24:00 UT. From 00:00 UT to 12:00 UT the next day, the X-component exhibited variations within −23 nT to 30 nT.

The eastward component of the geomagnetic field, Y, strength was observed to fluctuate within about −7 nT to 6 nT on the quiet days. From 10:00 UT to 24:00 UT on 23 April 2023, the level of strength fluctuations enhanced to ±20 nT. The following day, the Y-component strength showed variations within −27 nT to 15 nT over the interval 00:00 UT to 13:00 UT.

586
587 Generally, the vertical component of the geomagnetic field, Z, showed variations in strength smaller than ±3 nT.
588 Over the interval 10:00 UT on 23 April 2023 to 05:00 UT on 24 April 2023, a noticeable increase in the level of
589 strength fluctuations was recorded, down to –8 nT and up to ~10 nT.
590
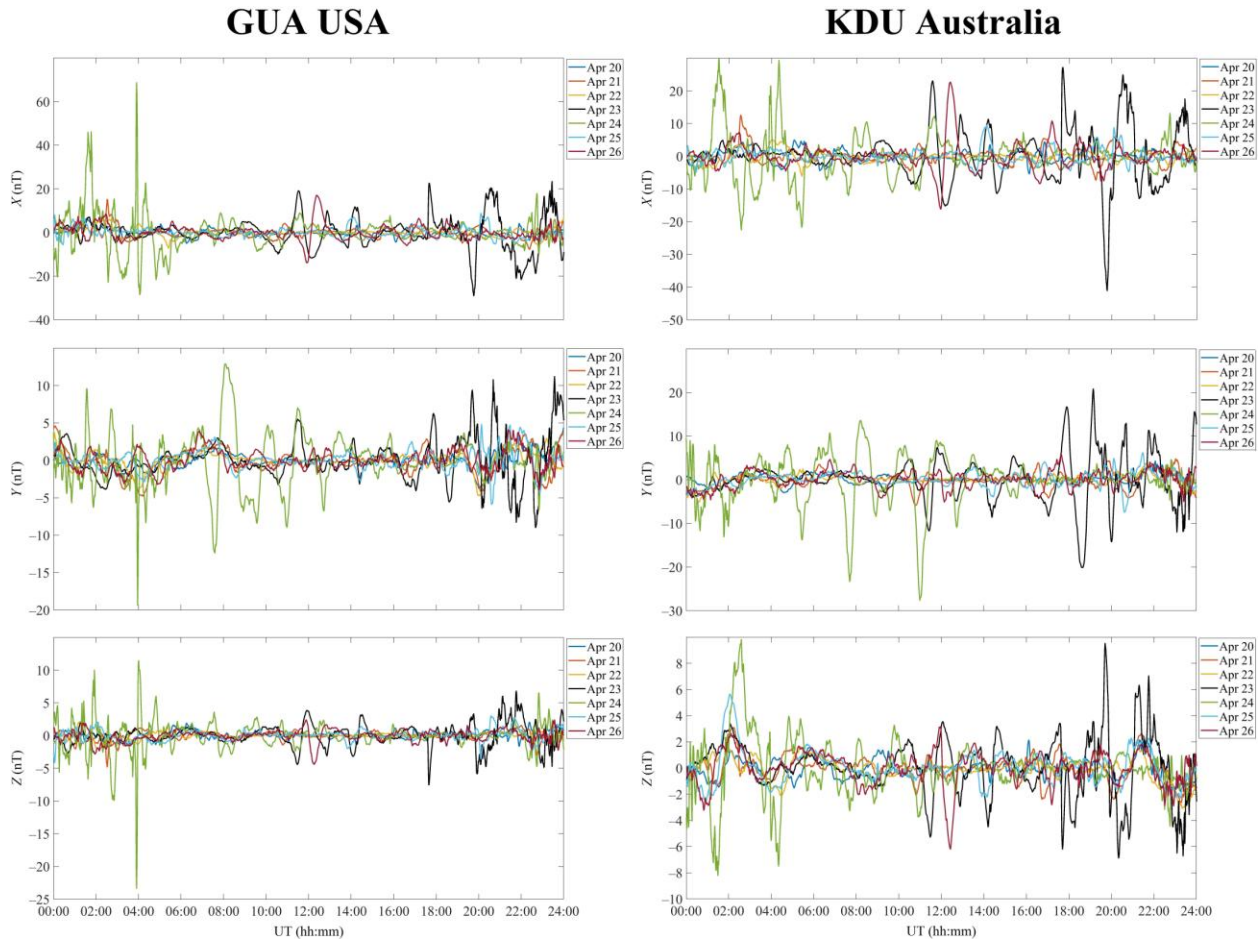
591
592
593 **Figure A.7: UT variations of the geomagnetic field at the GUA station (geographic coordinates 13.59°N, 144.87°E,**
594 **geomagnetic coordinates 6.10°N, 143.44°W) and at the KDU station (geographic coordinates 12.69°S, 132.47°E,**
595 **geomagnetic coordinates 20.96°S, 153.66°W) over the period 20–26 April 2023.**
596
597 *ASP Station*. The northward component of the geomagnetic field, X, showed the quiet time variability of strength
598 mainly within ±(3–10) nT (Fig. A.8). The enhancement in strength fluctuations with peak-to-peak amplitude of –53
599 nT to 32 nT was observed to occur between 10:00–24:00 UT on 23 April 2023, while between 00:00–06:00 UT the
600 next day, the X-component strength exhibited temporal variability within –28 nT to 39 nT.
601
602 During quiet days, the eastward component of the geomagnetic field, Y, exhibited strength variations smaller than
603 ±10 nT, which then significantly enhanced beginning at about 10:00 UT on 23 April 2023 and persisted until 13:00
604 UT on 24 April 2023. On the first day, the level of strength fluctuations was found between –33 nT and 43 nT, while
605 on the second day it varied from –44 nT to 15 nT.
606
607 On the days used as a quiet time reference period, the vertical component of the geomagnetic field, Z, exhibited
608 temporal variability within ±3 nT. From 10:00 UT to 24:00 UT on 23 April 2023, the Z-component showed an
609 increase in strength fluctuations from –6.5 nT to 5 nT, while on the following day it exhibited fluctuations from –5
610 nT to 12 nT.
611

612   *CNB Station*. On the quiet days, the northward component of the geomagnetic field, *X*, showed variations in strength
613   mainly from −10 nT to 10 nT (Fig. A.8). Significant enhancements in strength began at around 10:00 UT on 23
614   April 2023 and continued through to 12:00 UT on 24 April 2023. The strength of this component was observed to
615   vary from −62 nT to 55 nT on the first day, and within ±40 nT from 00:00 UT to 12:00 UT on the second day.
616
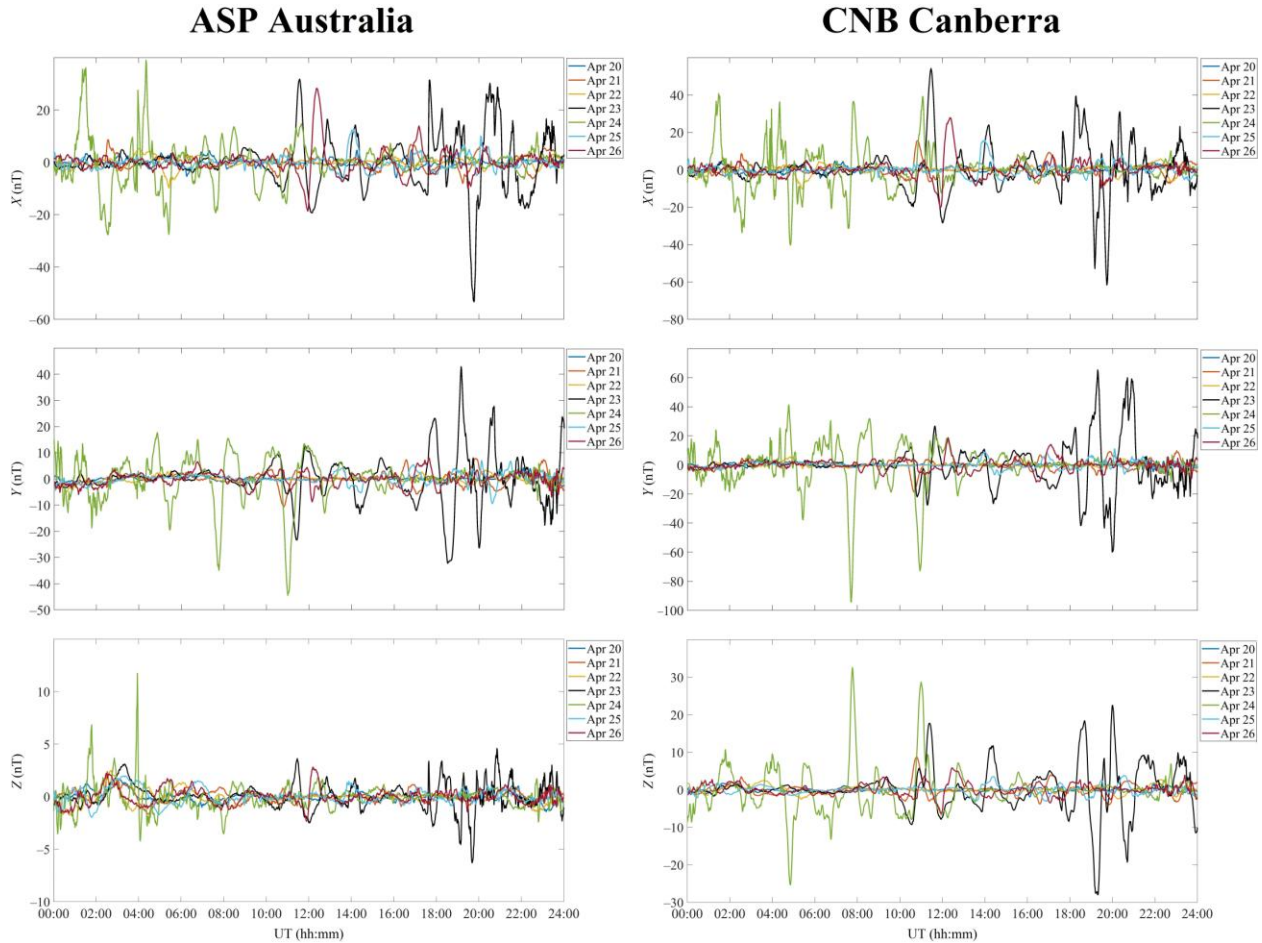
617
618
619   **Figure A.8: UT variations of the geomagnetic field at the ASP station (geographic coordinates 23.76°S, 133.88°E,**
620   **geomagnetic coordinates 31.83°S, 151.20°W) and at the CNB station (geographic coordinates 35.32°S, 149.36°E,**
621   **geomagnetic coordinates 41.75°S, 132.81°W) over the period 20–26 April 2023.**
622
623   On the days used as a quiet time reference period, the eastward component of the geomagnetic field, *Y*, showed
624   strength fluctuations not exceeding ±20 nT. Between 10:00 UT and 24:00 UT on 23 April 2023, the *Y*-component
625   exhibited variations in strength from −60 nT to 64 nT, and during the interval 00:00 UT to 12:00 UT on 24 April
626   2023, from −95 nT to 43 nT.
627
628   The vertical component of the geomagnetic field, *Z*, showed quiet time variations in strength smaller than ±8 nT.
629   Considerable enhancements in sharp variations in the strength of this component began at about 10:00 UT on 23
630   April 2023 and persisted until 12:00 UT on 24 April 2023, with the *Z*-component strength varying from −28 nT to
631   33 nT.
632
633   *MCQ Station*. On the quiet days, the northward component of the geomagnetic field, *X*, was observed to vary from −
634   40 nT to 70 nT (Fig. A.9), with the exception of a decrease by 380 nT and an increase by 200 nT in strength at
635   around 12:00 UT on 26 April 2023, as well as decreases by 160 nT and 120 nT at around 11:00 UT and 14:00 UT on
636   21 and 25 April 2023, respectively. Significant and sharp increases in amplitude and frequency fluctuations began at

637   10:00 UT on 23 April 2023 and stopped at around 12:00 UT on 24 April 2023, with the strength fluctuating within –
638   530 nT to 470 nT.

639

640   On the days used as a quiet time reference period, the eastward component of the geomagnetic field, Y, showed
641   variations in strength smaller than 30–40 nT, with the exception of a drop of about 200 nT that followed an increase
642   by 100 nT near 12:00 UT on 26 April 2023. A significant rise in amplitude and frequency fluctuations was observed
643   to occur after 10:00 UT on 23 April 2023 and continued until 12:00 UT on 24 April 2023, when the Y-component
644   strength varied from –600 nT to 340 nT.

645

646   Over the intervals 12:00–14:30 UT on 25 and 26 April 2023, the vertical component of the geomagnetic field, Z,
647   strength exhibited variability within –80 nT to 100 nT. On 21 April 2023, the strength reached 160 nT. In the course
648   of all other quiet days, this component showed variations not exceeding a few tens of nT. From 10:00 UT on 23
649   April 2023 to 12:00 UT on 24 April, the Z-component exhibited a sharp increase in temporal variability and the
650   level of strength fluctuations. The strength variations reached ±320 nT.

651

652   *CSY Station*. The northward component of the geomagnetic field, X, exhibited strength fluctuations generally
653   smaller than ±50 nT on the days used as a quiet time reference period (Fig. A.9). Sporadically, they reached ±100
654   nT. Significant variations began after 17:00 UT on 23 April 2023 and persisted for about 24 h. On 23 April 2023,
655   the strength of this component showed a decrease to –150 nT and increases to 100–110 nT. In the 24 April 2023
656   morning, the strength of this component showed variations within –100 nT to 160 nT. On the days used as a quiet
657   time reference period, the eastward component of the geomagnetic field, Y, showed variations usually not exceeding
658   ±(30–40) nT, whereas the strength fluctuations reached ±180 nT during the storm.

659

660   The vertical component of the geomagnetic field, Z, seldom exhibited variations in excess of 50 nT, with the greatest
661   variations (–380 nT to 260 nT) seen on 23 April 2023.

662

663   The particular attention should be given to significant, up to 300–380 nT, variations that were recorded in all
664   components from 12:40 UT to 16:00 UT on 24 April 2023. During this UT interval, the X-, Y-, and Z-components
665   exhibited strength fluctuations within –380–120 nT, –130–380 nT, and –250–290 nT, respectively.

666
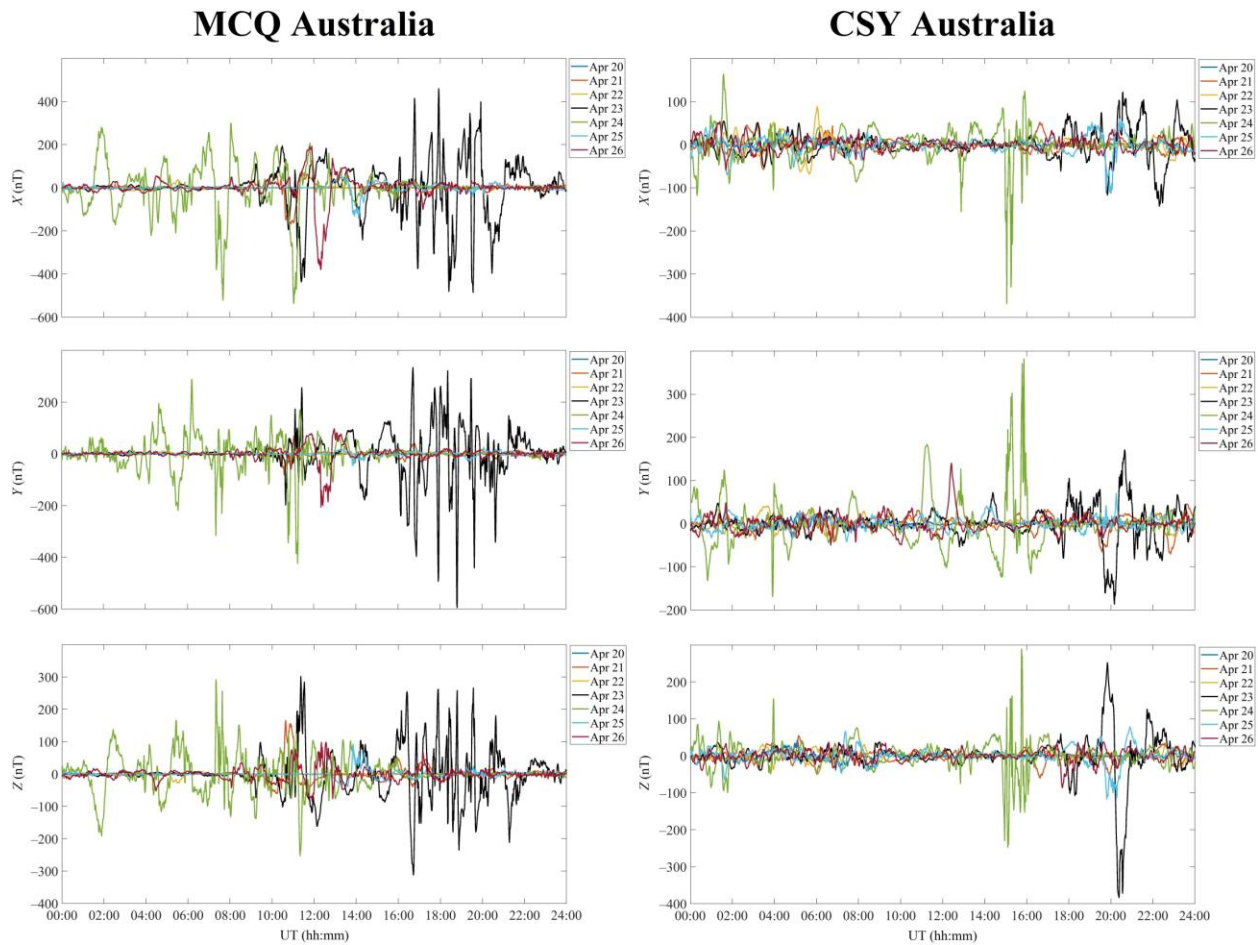
667
668
669 **Figure A.9: UT variations of the geomagnetic field at the MCQ station (geographic coordinates 54.5°S, 158.95°E,**
670 **geomagnetic coordinates 59.32°S, 116.38°W) and at the CSY station (geographic coordinates 66.283S, 110.5330E,**
671 **geomagnetic coordinates –75.53°S, –174.80°W).**

672 **Data Availability Statement**

673 The data sets discussed in this paper are freely accessible on the internet at https://imag-
674 data.bgs.ac.uk/GIN_V1/GINForms2.

675 **Author contributions**

676 **LC** processed the data observed, interpreted the physics of the observations and wrote the entire manuscript.

677 **Competing interests**

678 The contact author has declared that none of the authors has any competing interests.

679 **Acknowledgements**

680 This publication makes use of data collected by INTERMAGFNET and published at https://imag-
681 data.bgs.ac.uk/GIN_V1/GINForms2. The solar wind parameters have been retrieved from the Goddard Space Flight
682 Center Space Physics Data Facility https://omniweb.gsfc.nasa.gov/form/dx1.html. This research also draws upon
683 data provided by the World Data Center for Geomagnetism, Kyoto (data are retrieved from http://wdc.kugi.kyoto-
684 u.ac.jp). Special thanks are due to V. T. Rozumenko at V. N. Karazin Kharkiv National University who provided

685 useful comments on the contents of this paper. The author is grateful to his students M. B. Shevelev and Y. H.
686 Zhdanko for their assistance in preparing this paper. Support for L. F. Chernogor was also provided by Ukraine state
687 research projects # 0124U000478 and #0122U001476.

References

689 Abe, O. E., Fakomiti, M. O., Igboama, W. N., Akinola, O. O., Ogunmodimu, O., and Migoya-Orué, Y. O.:
690 Statistical analysis of the occurrence rate of geomagnetic storms during solar cycles 20–24, Adv. Space Res., 71,
691 2240–2251, https://doi.org/10.1016/j.asr.2022.10.033, 2023.

692 Al Shidi, Q., Pulkkinen, T., Toth, G., Brenner, A., Zou, S., and Gjerloev, J.: A large simulation set of geomagnetic
693 storms—Can simulations predict ground magnetometer station observations of magnetic field perturbations? Space
694 Weather, 20, e2022SW003049, 2Q, 2022.

695 Bothmer, V., and Daglis, I.: Space Weather: Physics and Effects, New York: Springer-Verlag,
696 https://doi.org/10.1007/978-3-540-34578-7, 2006.

697 Buonsanto, M.: Ionospheric storms — A review, Space Sci. Revs., 88, 563–601,
698 https://doi.org/10.1023/A:1005107532631, 1999.

699 CEDAR: The New Dimension, https://cedarscience.org/sites/default/files/2021-10/CEDAR_October_V9.2.pdf, last
700 access October 15, 2024, 2010.

701 Chernogor, L. F.: Physics of geospace storms, Space Science and Technology, 27, 3–77,
702 https://doi.org/10.15407/knit2021.01.003, 2021a.

703 Chernogor, L. F.: Statistical Characteristics of Geomagnetic Storms in the 24th Cycle of Solar Activity, Kinematics
704 and Physics of Celestial Bodies, 37, 193–199, https://doi.org/10.3103/S0884591321040048, 2021b.

705 Chernogor, L. F., and Domnin, I. F.: Physics of geospace storms, Kharkiv: V. N. Karazin Kharkiv National
706 University Publ., 2014.

707 Chernogor, L. F., Garmash, K. P., Guo, Q., and Zheng, Y.: Effects of the Strong Ionospheric Storm of August 26,
708 2018: Results of Multipath Radiophysical Monitoring, Geomagn. Aeron., 61, 73–91,
709 https://doi.org/10.1134/S001679322006002X, 2021.

710 Chernogor, L. F., Grigorenko, Ye. I., Lysenko, V. N., and Taran, V. I.: Dynamic processes in the ionosphere during
711 magnetic storms from the Kharkov incoherent scatter radar observations, Int. J. Geomagn. Aeron., 7, GI3001,
712 https://doi.org/10.1029/2005GI000125, 2007.

713 Chernogor, L. F., and Shevelev, M. B.: Latitudinal dependence of quasi-periodic variations in the geomagnetic field
714 during the greatest geospace storm of September 7-9, 2017. Space Sci. and Technol, 26, 72–83,
715 https://doi.org/10.15407/knit2020.02.072, 2020.

716 Daglis, I. A.: Space Storms and Space Weather Hazards, New York: Springer Dordrecht,
717 https://www.springer.com/gp/book/9781402000300, 2001.

718 Danilov, A. D., and Laštovička, J.: Effects of geomagnetic storms on the ionosphere and atmosphere. Int. J.
719 Geomag. Aeron., 2, 209–224, https://elpub.wdcb.ru/journals/ijga/v02/gai99312/gai99312.htm, 2001.

720 De Abreu, A. J., Correia, E., De Jesus, R., Venkatesh, K., Macho, E. P., and Roberto, M.: Statistical analysis on the
721 ionospheric response over South American mid- and near high-latitudes during 70 intense geomagnetic storms
722 occurred in the period of two decades, Journal of Atmospheric and Solar-Terrestrial Physics, 245, 106060,
723 https://doi.org/10.1016/j.jastp.2023.106060, 2023.

724 Fagundes, P. R., Tsali-Brown, V. Y., Pillat, V. G., Arcanjo, M. O., Venkatesh, K., and Habarulema, J. B.:
725 Ionospheric storm due to solar Coronal mass ejection in September 2017 over the Brazilian and African longitudes,
726 Advances in Space Research, 71, 46–66, https://doi.org/10.1016/j.asr.2022.07.040, 2023.

727 Fuller-Rowell, T. J., Codrescu, M. V., Roble, R. G., and Richmond, A. D.: How does the thermosphere and
728 ionosphere react to a geomagnetic storm? Magnetic storms, in: Geoph. Monog. Series, edited by Tsurutani B. T.,
729 Gonzalez W. D., Kamide Y., Arballo J. K., 98, 203–226, https://doi.org/10.1029/GM098p0203, 1997.

730 Ghag, K., Raghav, A., Bhaskar, A., Soni, S. L., Sathe, B., Shaikh, Z., Dhamane, O., and Tari, P.: Quasi-planar
731 ICME sheath: A cause of first two-step extreme geomagnetic storm of 25th solar cycle observed on 23 April 2023,
732 Advances in Space Research, 73(12), 6288–6297, DOI:10.1016/j.asr.2024.03.011, 2024.

733 Gonzalez, W. D., Jozelyn, J. A., Kamide, Y., Kroehl, H. W., Rostoker, G., Tsurutani, B. T., and Vasyliunas, V. M.:
734 What is a geomagnetic storm? J. Geophys. Res., 99, 5771–5792, https://doi.org/10.1029/93JA02867, 1994.

735 Hsu, C.-T., and Pedatella, N. M.: Effects of forcing uncertainties on the thermospheric and ionospheric states during
736 geomagnetic storm and quiet periods, Space Weather, 21, e2022SW003216,
737 https://doi.org/10.1029/2022SW003216, 2023.

Kamide, Y., and Maltsev, Y. P.: Geomagnetic Storms. In: Kamide, Y., Chian, A. (Eds.) Handbook of the Solar-Terrestrial Environment., Berlin, Heidelberg: Springer-Verlag, 355–374, https://doi.org/10.1007/978-3-540-46315-3_14, 2007.

Katsko, S. V., Emelyanov, L. Ya., and Chernogor, L. F.: Features of the Ionospheric Storm on December 21-24, 2016, Kinematics and Physics of Celestial Bodies, 37, 85–95, https://doi.org/10.3103/S0884591321020045, 2021.

Kepko, L., McPherron, R.L., Amm, O., Apatenkov, S., Baumjohann, W., Birn, J., Lester, M., Nakamura, R., Pulkkinen, T.I., and Sergeev, V.: Substorm Current Wedge Revisited, Space Sci. Rev., 190, 1–46, https://doi.org/10.1007/s11214-014-0124-9, 2015.

Kleimenova, N. G., Kozyreva, O. V., Michnowski, S., and Kubicki, M.: Effect of magnetic storms in variations in the atmospheric electric field at midlatitudes, Geomagn. Aeron., 48, 622–630, https://doi.org/10.1134/S0016793208050071, 2008.

Kleimenova, N.G., Kubicki, M., Odzimek, A., Malysheva, L. M., and Gromova L. I.: Effects of geomagnetic disturbances in daytime variations of the atmospheric electric field in polar regions, Geomagn. Aeron., 57, 266–273, https://doi.org/10.1134/S0016793217030070, 2017.

Koskinen, H. E. J.: Physics of space storms. From Solar Surface to the Earth, Berlin, Heidelberg: Springer-Verlag, https://doi.org/10.1007/978-3-642-00319-6, 2011.

Laskar, F. I., Sutton, E. K., Lin, D., Greer, K. R., Aryal, S., and Cai, X.: Thermospheric temperature and density variability during 3-4 February 2022 minor geomagnetic storm, Space Weather, 21, e2022SW003349, https://doi.org/10.1029/2022SW003349, 2023.

Laštovička, J.: Effects of geomagnetic storms in the lower ionosphere, middle atmosphere and troposphere. *J. Atmos. Terr. Phys*., *58*, 831–843, https://doi.org/10.1016/0021-9169(95)00106-9, 1996.

Lin, D., Wang, W., Merkin, V. G., Huang, C., Oppenheim, M., and Sorathia, K.: Origin of dawnside subauroral polarization streams during major geomagnetic storms. AGU Advances, 3, e2022AV000708, https://doi.org/10.1029/2022AV000708, 2022.

Luo, Y., Chernogor, L. F., Garmash, K. P., Guo, Q., Rozumenko, V. T., and Zheng, Y.: Dynamic processes in the magnetic field and in the ionosphere during the 30 August-2 September 2019 geospace storm: influence on high frequency radio wave characteristics, Ann. Geophys., 39, 657–685, https://doi.org/10.5194/angeo-39-657-2021, 2021a.

Luo, Y., and Chernogor, L. F.: Characteristic Features of the Magnetic and Ionospheric Storms on December 21–24, 2016, Kinematics and Physics of Celestial Bodies, 38, 262–278, https://doi.org/10.3103/S0884591322050051, 2022.

Luo, Y., Chernogor, L. F., and Garmash, K. P.: Magneto-Ionospheric Effects of the Geospace Storm of March 21-23, 2017, Kinematics and Physics of Celestial Bodies, 38, 210–229, https://doi.org/10.3103/S0884591322040055, 2022.

Luo, Y., Guo, Q., Zheng, Y., Garmash, K. P., Chernogor, L. F., and Shulga, S. N.: Geospace storm effects on August 5-6, 2019 (in Ukrainian), Space Science and Technology, 27, 45–69, https://doi.org/10.15407/knit2021.02.045, 2021b.

Moldwin, M.: An introduction to space weather (2nd ed.), Cambridge: Cambridge University Press, https://doi.org/10.1017/9781108866538, 2022.

Oikonomou, C., Haralambous, H., Paul, A., Ray, S., Alfonsi, L., Cesaroni, C., and Sur, D.: Investigation of the negative ionospheric response of the 8 September 2017 geomagnetic storm over the European sector, Advances in Space Research, 70, 1104–1120, https://doi.org/10.1016/j.asr.2022.05.035, 2022.

Prölss, G. W.: Ionospheric F-region storms, in: Handbook of Atmospheric Electrodynamics, edited by Volland H., Florida, USA: CRC Press, Boca Raton, https://doi.org/10.1201/9780203713297, 2, 195–248, 1995.

Prölss, G. W., and Roemer, M.: Thermospheric storms, Adv. Space Res., 7, 223–235, https://doi.org/10.1016/0273-1177(87)90096-2, 1987.

Qian, L., Wang, W., Burns, A. G., Chamberlin, P. C., Coster, A., Zhang, S.-R., and Solomon, S. C.: Solar flare and geomagnetic storm effects on the thermosphere and ionosphere during 6-11 September 2017, Journal of Geophysical Research: Space Physics, 124, 2298–2311, https://doi.org/10.1029/2018JA026175, 2019.

Song, P., Singer, H., and Siscoe, G. (Eds.): Space Weather, Geophysical Monograph, Washington, DC: American Geophysical Union, https://doi.org/10.1002/9781118668351, 2001.

Tariq, M. A., Yuyan, Y., Shah, M., Shah, M. A., Iqbal, T., and Liu, L.: Ionospheric-Thermospheric responses to the May and September 2017 geomagnetic storms over Asian regions, Adv. Space Res., 70, 3731–3744, https://doi.org/10.1016/j.asr.2022.08.050, 2022.

Wen, D., and Mei, D.: Ionospheric TEC disturbances over China during the strong geomagnetic storm in September 2017, Adv. Space Res., 65, 2529–2539, https://doi.org/10.1016/j.asr.2020.03.002, 2020.

793   Wang, J., Yang, C., and An, W.: Regional Refined Long-term Predictions Method of Usable Frequency for HF
794   Communication Based on Machine Learning over Asia, IEEE Trans. Antennas Propag., 70, 4040–4055, DOI:
795   10.1109/TAP.2021.3111634, 2022.
796   Wang, J., Shi, Y., Yang, C., Zhang, Z., and Zhao, L.: A Short-term Forecast Method of Maximum Usable Frequency
797   for HF Communication, IEEE Trans. Antennas Propag., 71, 5189–5198, DOI:10.1109/TAP.2023.3266584, 2023.